nature nanotechnology

Article

https://doi.org/10.1038/s41565-022-01287-x

Simultaneous identification of viruses and viral variants with programmable DNA nanobait

Received: 2 November 2021

Accepted: 7 November 2022

Published online: 16 January 2023

Check for updates

Filip Bošković[1], Jinbo Zhu[1], Ran Tivony[1], Alexander Ohmann[1], Kaikai Chen[1], Mohammed F. Alawami[1], Milan Đorđević[1], Niklas Ermann[1], Joana Pereira-Dias[2,3], Michael Fairhead[4], Mark Howarth[4], Stephen Baker[2,3] & Ulrich F. Keyser[1]

Respiratory infections are the major cause of death from infectious disease worldwide. Multiplexed diagnostic approaches are essential as many respiratory viruses have indistinguishable symptoms. We created self-assembled DNA nanobait that can simultaneously identify multiple short RNA targets. The nanobait approach relies on specific target selection via toehold-mediated strand displacement and rapid readout via nanopore sensing. Here we show that this platform can concurrently identify several common respiratory viruses, detecting a panel of short targets of viral nucleic acids from multiple viruses. Our nanobait can be easily reprogrammed to discriminate viral variants with single-nucleotide resolution, as we demonstrated for several key SARS-CoV-2 variants. Last, we show that the nanobait discriminates between samples extracted from oropharyngeal swabs from negative- and positive-SARS-CoV-2 patients without preamplification. Our system allows for the multiplexed identification of native RNA molecules, providing a new scalable approach for the diagnostics of multiple respiratory viruses in a single assay.

The diagnosis of infectious diseases plays a vital role in determining appropriate patient treatment[1]. Respiratory tract infections are the major cause of death from infectious diseases globally[2,3]. Many respiratory viruses induce comparable symptoms and cannot be clinically differentiated, making the identification of appropriate treatment challenging. It is estimated that 65% of infection-associated cases of pneumonia are potentially misdiagnosed, with 95% of these cases erroneously receiving antimicrobials[4]. The ongoing coronavirus disease 2019 (COVID-19) pandemic further highlights another unmet diagnostic need: the routine identification and screening of viral variants as they arise[5].

Currently, viral diagnostics rely on quantitative reverse transcription–polymerase chain reaction (qRT-PCR), followed by genome sequencing, to detect viral variants[5,6]. Polymerase-chain-reaction-based diagnostic methods provide a sensitive approach for detecting viral nucleic acids in complex biological samples but suffer from limited multiplexing capabilities[7]. There is a need for robust diagnostic methods that can simultaneously detect multiple respiratory viruses and variants in a limited sample volume, which can be quickly reconfigured to detect additional variants as they arise. Newer nucleic acid detection methods, such as nanopore sensing, which can distinguish multiple nucleic acid species[8–11] with a unique signature for each designed DNA

[1]Cavendish Laboratory, University of Cambridge, Cambridge, UK. [2]University of Cambridge School of Clinical Medicine, Cambridge Biomedical Campus, Hills Road, Cambridge, UK. [3]Department of Medicine, University of Cambridge School of Clinical Medicine, Cambridge Biomedical Campus, Hills Road, Cambridge, UK. [4]Department of Biochemistry, University of Oxford, Oxford, UK. e-mail: ufk20@cam.ac.uk

nanostructure may be an alternative approach for multiplexed biosensing[12–14]. Various groups have shown that nanopore sensing after viral nucleic acid enrichment or amplification may be a suitable platform to challenge these diagnostics[10,15,16].

Here, aiming to solve many of the limitations for diagnostic multiplexing, we developed an innovative method that employs a bespoke nanobait for the simultaneous identification of multiple respiratory viruses and variants[17]. We employed programmable viral RNA cutting with ribonuclease (RNase) H to remove short RNA targets that uniquely identify the virus. The resultant RNA target is captured by the nanobait, which is immediately detected by nanopore sensing, without reverse transcription, preamplification or purification. By multiplexing several targets from the same virus in samples containing human RNA, we show that our method can increase specificity and throughput compared with existing platforms, and can pave the way for amplification-free RNA identification and diagnostics.

Single-molecule target RNA detection with nanobaits

We developed a workflow for the nanobait detection of target RNA, ranging from patient swabbing, nucleic acid extraction and programmable RNase H cutting of viral RNA (Fig. 1). The RNA targets are selected by guide oligonucleotides (single-stranded DNA, 20 nt) that were designed to bind upstream and downstream on the specific regions in a viral genome. Then, RNase H was used to digest the RNA sequence in RNA: DNA hybrids (DNA guide oligo hybridized to viral RNA segment) and release the middle target RNA (Fig. 1a, right).

The released RNA targets were identified using sequence-specific binding to the nanobait (Fig. 1b,c). The nanobait was designed (Supplementary Fig. 1) with five binding sites that could incorporate up to five targets. The nanobait was assembled by mixing a single-stranded DNA scaffold (linearized M13mp18, 7,228 nt long)[12] with a collection of short complementary oligonucleotides (Fig. 1b, Supplementary Fig. 1 and Supplementary Table 2). Towards one end of the nanobait, the sensing region was designed to contain equally spaced sites a–e flanked by two reference structures R1 and R2, which consisted of six DNA dumbbells each (Supplementary Table 3 lists the oligonucleotides). The sensing site contained a DNA overhang, which was fully complementary to the respective target sequence. We additionally exploited a blocking oligo with a label (monovalent streptavidin[18] or DNA flower; Supplementary Fig. 2 and Supplementary Table 1) that was only partially hybridized and left six bases unpaired. The assembly of the nanobait was confirmed by atomic force microscopy (AFM) imaging and electrophoretic mobility shift assay (Supplementary Figs. 3–5). Ultimately, if the target was present, it would bind to the six unpaired bases and displace the blocking oligo with the label at its complementary overhang, which is known as toehold-mediated strand displacement[19]. Hence, the presence of the predefined targets was indicated by the absence of a label at the respective site (Fig. 1c,d).

We determined the structure of each nanobait and ability to detect the presence or absence of targets by a single-molecule readout technique exploiting nanopore resistive pulse sensing (Fig. 1e–g). Nanopore DNA sensing works via the voltage-driven translocation of negatively charged nanobaits through a small orifice towards a positively charged electrode in an electrolyte solution (Fig. 1e)[20]. Here the nanobait translocation induces a unique current blockage signature (Fig. 1f). The first current drop corresponded with double-stranded DNA nanobait (ΔI_{DNA}). The second current drop (ΔI_{label}) indicated the presence of references R1 and R2 and labels a–e (Fig. 1c). Figure 1f depicts an example of a nanobait–nanopore event with seven downward spikes, where each spike corresponds to the matching colour site in the schematic shown in Fig. 1c. After strand displacement with all the five targets present (Fig. 1d, a′–e′), the five labelled oligos were displaced and only the reference spikes remain (Fig. 1g). The short duplexes were significantly smaller than the labels and not detected with these nanopores[21]. Each ionic current event on a single nanobait revealed the presence of multiple short RNA targets. The flexibility of the nanobait design permitted us to identify targets originating from multiple parts of the same virus or from multiple viral genomes.

Simultaneous detection of multiple viral variants

We designed the nanobait for the multiplexed target identification of SARS-CoV-2, respiratory syncytial virus (RSV) (universal for group A), rhinovirus (universal), influenza (universal for group A) and parainfluenza 1 (Supplementary Tables 4–7). A schematic of the nanobait design for multiple respiratory viral nucleic acid targets is shown in Fig. 2a. RSV is provided as an example of site-specific displacement (Fig. 2a). The five targets, as well as the control (no target), were independently detected using the same nanobait. The first nanopore translocation events of the nanobait in each of the individual samples are depicted in Fig. 2a and Supplementary Fig. 6. Nanopore events with seven spikes indicated the absence of targets. If the respective target for SARS-CoV-2, RSV, rhinovirus, influenza or parainfluenza were present, that spike was absent in the nanobait translocation event (Supplementary Table 4 lists the presence of targets). The displacement efficiency was calculated as the difference between a no-target control and the measurement for each site (50 nanobait events for each of the three nanopore recordings) (***$p < 0.001$; two-sided Student's t-test) (Fig. 2c). We tested two different scenarios, with and without targets, for statistical significance.

Variant discrimination with single-nucleotide resolution is an essential feature for variant diagnostics. We tested the potential of the nanobait for the discrimination of a single-nucleotide variant by distinguishing nucleic acids from several SARS-CoV-2 variants. The five sites of nanobait allowed for the simultaneous detection of wild-type (WT) virus and four variants (Supplementary Tables 8–12 list the sequences and Supplementary Section 7 elaborate the design principles)[22]. The first site was WT SARS-CoV-2 isolated in Wuhan (B as per the PANGOLIN nomenclature)[22]. The alternative four targets were European strain B.1 and three variants of concern[17], namely, B.1.1.7 (Alpha), B.1.351 (Beta) and B.1.617 (Delta), which were first detected in the United Kingdom, South Africa and India, respectively. As an example, we highlight the identification of the B.1.1.7 variant (Fig. 2d). We selected a variant-specific target that was fully complementary to the capture strand on the nanobait, whereas the WT target contained a mismatch in the toehold end (Supplementary Table 11). The displacement efficiency is dependent on the number and position of mismatches in the toehold domain[23]. Programming the nanobait with a single-nucleotide mismatch allowed us to discriminate the SARS-CoV-2 variant from the WT sequence. We depict example events for each sample where all the spikes are present (no targets) or the respective spike is absent depending on which variant is present (Fig. 2e; Supplementary Fig. 7 shows more events and Supplementary Table 8 lists the presence of targets). Figure 2f shows the displacement efficiency for WT targets and their corresponding variant targets for the first 50 nanobait events (coloured bars). We observed a significant difference for all the four variants compared with the respective WT samples (light- and dark-coloured bars). In addition, we demonstrated the principle by using two single-nucleotide SARS-CoV-2 RNA viral variants (Supplementary Fig. 8 and Supplementary Section 8).

Identification of multiple SARS-CoV-2 targets

Diagnostic tests for viral RNA rely on multistep reactions and subsequent purification steps. We aimed to use nanobait for direct target identification without preamplification and purification. Here we used the nanobait for the specific single-molecule detection in a complex human transcriptome mixture that is human total RNA (htRNA; Invitrogen). These nanobaits could identify multiple samples from pooled samples in complex backgrounds by nanopore sensing (Fig. 3a).

https://doi.org/10.1038/s41565-022-01287-x

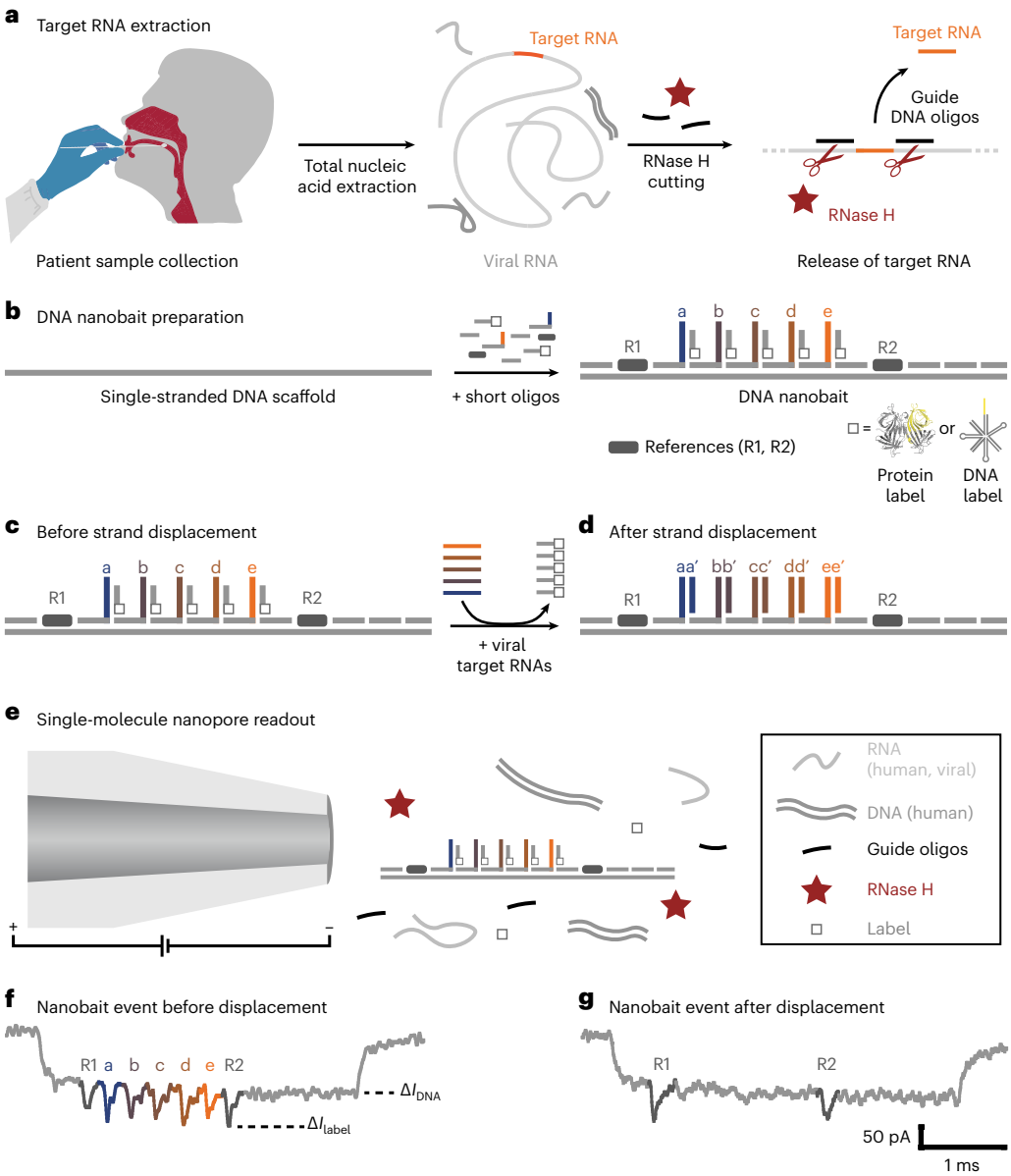

Fig. 1 | Self-assembled DNA nanobait strategy for multiplexed viral diagnostics. a, Oropharyngeal swab sample is collected from patients suspected to have COVID-19. The total nucleic acids were extracted (human and viral RNAs are shown in light grey; DNA is shown in dark grey), and the target RNA was cleaved out using programmable RNase H cutting. Such a treated sample was further tested for viral presence. **b**, Nanobait is made by mixing a single-stranded DNA scaffold (M13mp18 DNA) with short oligonucleotides where some of them carry complementary capture strands (a–e) for specific targets (a′–e′) in a target viral RNA. In addition, a partially complementary oligo with a structural label (protein or DNA based; white square) is added to each site to amplify the signal in nanopore recordings. We marked a sensing region with two references (dark grey). **c**,**d**, Nanobait before (**c**) and after (**d**) strand displacement reactions of five targets (coloured strands). If the targets are present, the five grey strands with labels are displaced. The two outer signals originate from reference structures that indicate the sensing region, and the five binding sites between the references are specific for the five different targets. **e**, Each nanobait is voltage driven through the nanopore and detected in a mixture of molecules. **f**, Typical nanopore current signature as a function of time for a nanobait as designed with five labels present. The first current drop corresponds to DNA (ΔI_{DNA}) and the second to labels (ΔI_{label}). **g**, Typical nanobait event after strand displacement of all the five targets. The presence of targets is detected by the missing downward signals specific to each target.

We pooled together five synthesized SARS-CoV-2 RNA targets to investigate the specificity and potential crosstalk between the nanobait and non-specific htRNA background. After the targets were added, all the sites were displaced and correctly identified using the nanopore measurements (Fig. 3b). A typical current trace indicates that nanobait spikes can be easily distinguished (Fig. 3c, red boxes) from non-specific current blockages originating from the htRNA. Figure 3d,e shows the first five linear nanobait events for samples with and without targets and in the presence of htRNA; the displacement efficiency for all the five targets is depicted in Fig. 3f. Target 4 had the lowest displacement efficiency, which was in agreement with a low predicted guanine-cytosine (GC) content of 25% (ref. 24). Nanobait-based strand displacement can effectively operate even in a complex background of htRNA, oligonucleotides and proteins. We studied the kinetic details for both RNA and DNA targets and determined that 10 min was the optimal incubation time for the strand displacement reaction (Supplementary Section 9 provides the corresponding plots and events, Supplementary Table 14 lists the presence

https://doi.org/10.1038/s41565-022-01287-x

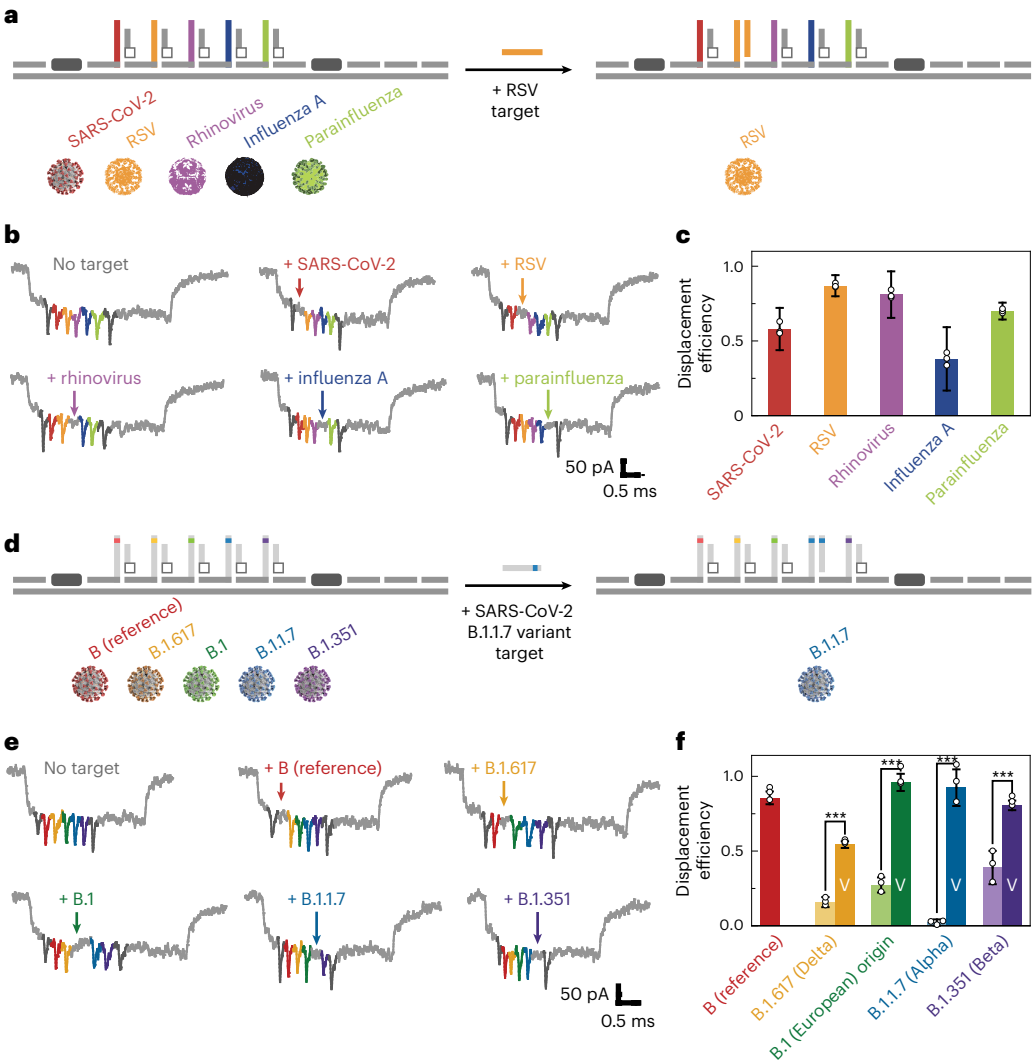

Fig. 2 | Multiplexed discrimination of viruses and SARS-CoV-2 variants with nanobait. a, Nanobait is designed to have five sites specific to SARS-CoV-2, RSV, rhinovirus, influenza A and parainfluenza. **b**, Example events for the condition without any targets and for each virus-specific target. The absence of the coloured spike indicates the presence of each respective target. **c**, Displacement efficiency indicates the presence of the corresponding viral target. The displacement efficiency represents a measurement with the target subtracted from the control (no targets). The error bars represent the standard error and the centre is the mean for three nanopore measurements and 50 nanopore events per measurement. **d**, Nanobait designed to detect four single-nucleotide SARS-CoV-2 variants by adaptation of the target sequences. **e**, Example events for the condition without any targets and for each variant-specific target are depicted. The absence of the coloured spike indicates the presence of each respective variant. **f**, Displacement efficiencies for single-nucleotide variants (labelled as 'V') are compared with the displacement efficiency for the WT strain of the SARS-CoV-2 virus isolated in Wuhan. The error bars represent the standard error and the centre is the mean for three nanopore measurements and 50 nanopore events per measurement. The difference between the conditions without and with the variant targets is statistically significant (***$p < 0.001$; two-sided Student's t-test; $N = 150$).

of targets and Supplementary Tables 15–17 list the target sequences and oligonucleotides).

Design of target sites depends on viral RNA secondary structure

We next aimed to optimize multiple parameters in designing an efficient target RNA identification system. One key parameter was the successful excision of the short RNA targets from viral RNA. We found that the location of the target RNA in the viral RNA secondary structure affected the concentration of free target RNA and consequently affected the displacement efficiency. A target in a highly complementary region would remain bound to the viral RNA after cutting and prevent detection. In contrast, the release of the target after RNase H excision increases when more unpaired bases were in the target region than within the secondary structure of the viral RNA. For future experiments, we can maximize the number of unpaired bases to increase the effective concentration of the target in solution and consequently aid detection.

The role of unpaired bases was demonstrated by the detection of three targets in the ~3.6 kb RNA genome of the MS2 virus (Fig. 4a shows the minimal free energy secondary structure[25]). The three targets (T1, T2 and T3) had a decreasing percentage of unpaired bases (T1, 55%; T2, 30%; and T3, 25%). Subsequently, we designed oligos and employed RNase H cutting of all the three targets and quantified the displacement efficiency using nanobait with the three sites (Fig. 4b; Supplementary Fig. 15 shows more events, Supplementary Table 18 lists the presence of targets and Supplementary Tables 19–23 list the oligonucleotides). Efficient cutting of viral RNA was confirmed by agarose gel electrophoresis (Supplementary Fig. 11). For each target, the original 3.6 kb

https://doi.org/10.1038/s41565-022-01287-x

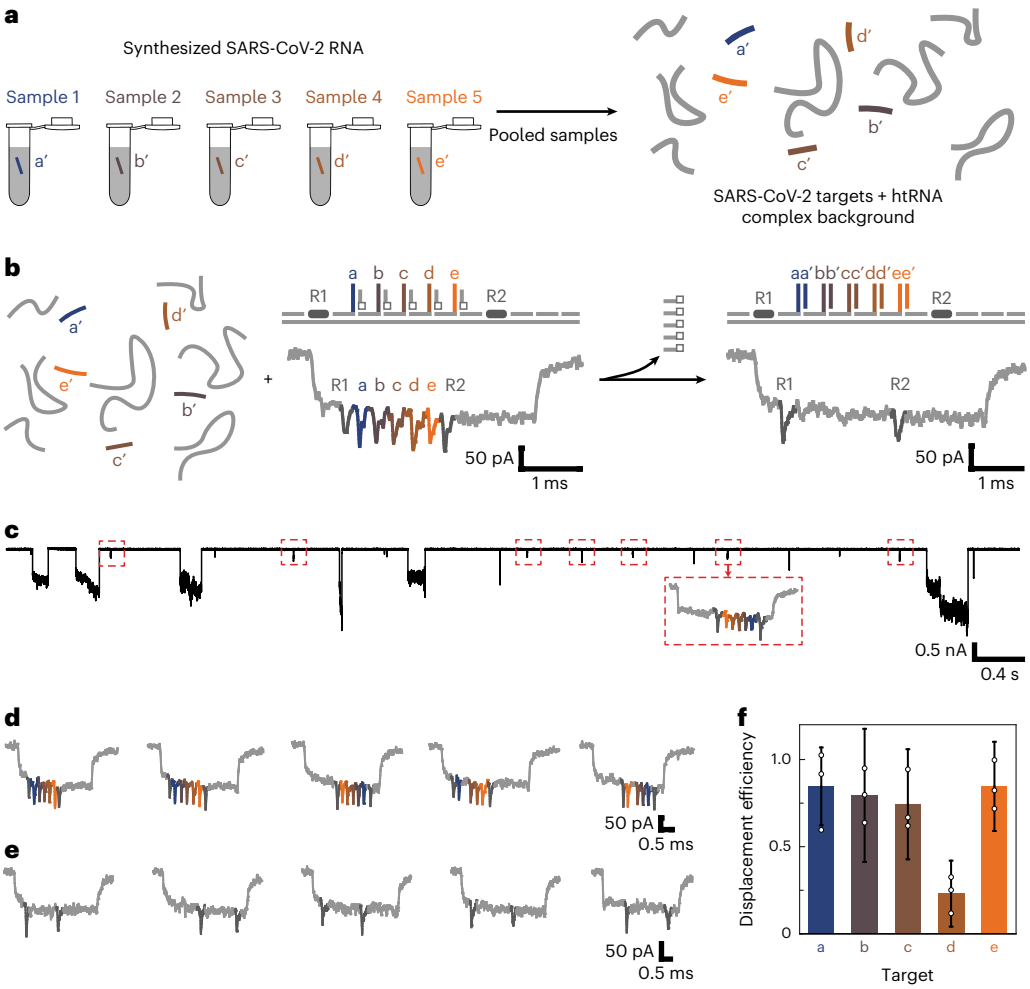

Fig. 3 | Nanobait detects multiple synthesized SARS-CoV-2 RNA targets in the background of human transcriptional RNA. a, Five targets from different regions in a viral genome can be separately targeted and pooled for nanopore analysis. The five targets are mixed with intact htRNA in the background to verify that viral RNA purification is not a required step. **b**, After the addition of a nanobait to the mix, all the five targets can be identified in parallel, as shown in the example events. **c**, Ionic current traces indicate the specificity of the method for the identification of nanobait-specific events even in a complex background where large downward signals originate from the background including long RNAs. All the nanobait events have been highlighted in the red dashed boxes. **d**, First five single-file nanobait events for the sample mixed with only htRNA indicate the correct current signature. **e**, First five single-file nanobait events that have been previously mixed with the targets and htRNA. All the targets are present since the corresponding spikes are absent in the nanopore events. **f**, Displacement efficiency calculated for the sample with targets added (nanobait with targets and htRNA) for all the five sites. The error bars represent the standard error and the centre is the mean for three nanopore measurements and 50 nanopore events per measurement.

RNA was cut into fragments of the predicted length; additionally, the predicted fragment lengths were comparable when all the three targets were simultaneously cut. We confirmed that target T1 was free in solution by hybridizing it to the complementary capture of strand C and detecting it using polyacrylamide gel electrophoresis (Fig. 4c). After cutting, target T2 was not visible by polyacrylamide gel electrophoresis (Supplementary Fig. 14), and the oligonucleotides' running speed and non-specific interactions were validated on control polyacrylamide gel electrophoresis (Supplementary Figs. 12 and 13).

Example nanopore events and displacement efficiency with and without the targets released from the MS2 RNA genome after RNase H cutting are shown in Fig. 4b,d. The plot indicates that displacement was detected for all the three targets. Target T1 had the highest displacement efficiency, whereas target T3 had the lowest displacement efficiency. As predicted, the displacement efficiency (Fig. 4d) correlated with the unpaired base percentage in the RNA structure for each target, signifying an important design principle in selecting the viral target regions for detection.

Amplification-free SARS-CoV-2 identification in clinical samples

After establishing that RNase H had cut the MS2 RNA, we considered that the nanobait could detect SARS-CoV-2 RNA in clinical samples. We accessed oropharyngeal swabs from patients suspected to have COVID-19; the viral load of SARS-CoV-2 in oropharyngeal swabs in the clinical phase can be up to 10^8–10^{11} copies[13,14]. The sensitivity curve for nanopore readout was plotted (Supplementary Section 16 and Supplementary Fig. 19). We used the nanobait in nucleic acid extractions from clinical samples that had been prepared for qRT-PCR (Supplementary Section 12; Supplementary Tables 24–27 list the oligos)[26]. SARS-CoV-2 targets (S1, S2 and S3) were designed in the conserved regions of the genome that contained the highest percentage of unpaired bases (Fig. 5a). S1 was in the region encoding the spike (S) protein, S2 was in the region encoding the small envelope (E) glycoprotein and S3 was in the nucleocapsid (N) protein-coding region. The total nucleic acids from the clinical samples were subjected to our RNase H protocol (Fig. 5b) and then mixed with a nanobait with sensing sites S1, S2 and S3. The reaction

https://doi.org/10.1038/s41565-022-01287-x

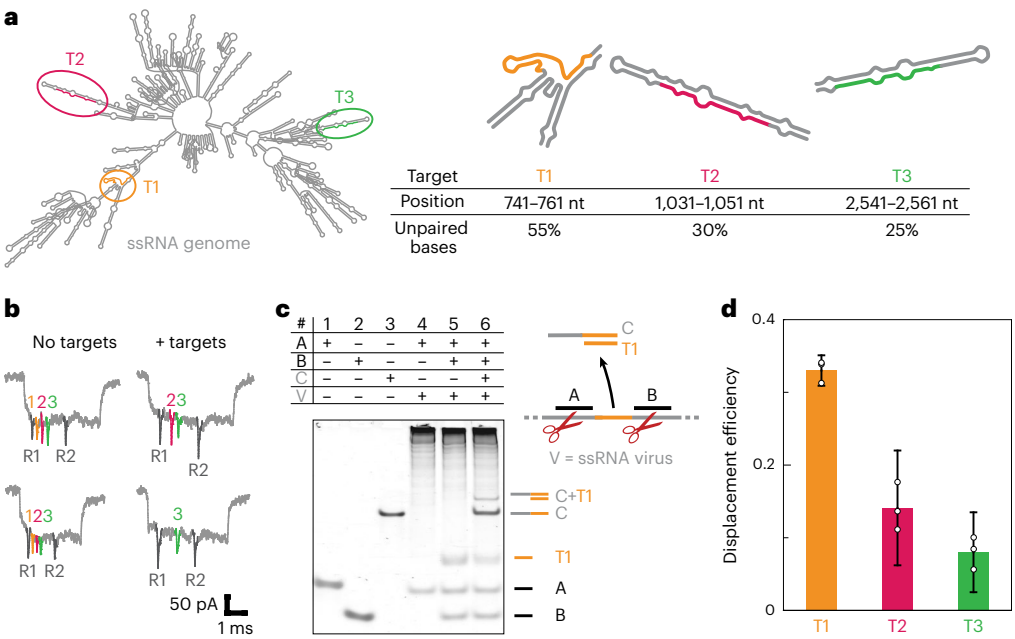

Fig. 4 | Position of a target in a viral RNA secondary structure influences the efficiency of target identification. a, We demonstrated that the position of a target in viral RNA correlates with the efficiency of target release after RNase H cutting. MS2 viral RNA is presented as the minimal free energy structure. Three targets (T1, T2 and T3) are selected to have different levels of paired bases for a constant 20-nt-long target. For each target, a region in the MS2 viral RNA is indicated with the percentage of unpaired bases in each target. **b**, Nanobait events with three targets present are shown, indicating the correct design (no targets). The events for the sample where the long RNA is mixed with the nanobait show displacement (+ targets). Each spike colour corresponds to a site on the nanobait. **c**, Electrophoretic mobility shift assay shows guide oligos A and B (lanes 1 and 2, respectively) and complementary oligo C to target T1 (lane 3). If only guide oligo A is used for viral RNA cutting (lane 4), there is only the oligo A band and the high-molecular-weight cut viral RNA. Once both guide oligos are added, an additional band originating from the released target T1 RNA emerges (lane 5). Once strand C is added to the same sample, we can see its shift after T1 binding (lane 6). **d**, Displacement efficiency of target RNAs correlates with the percentage of unpaired bases in a target. T1 shows the highest displacement, whereas T2 and T3 show lower displacement efficiencies. The error bars represent the standard error and the centre is the mean for three nanopore measurements and 50 nanopore events per measurement.

did not require further purification or preamplification before nanopore readout. The nanobait mixture was then analysed with nanopores containing the complex background of DNA (human and optionally DNA flower), long RNAs (human and potentially viral), short guide oligos and proteins (RNase H and monovalent streptavidin).

Nanopore events from the nanobait mixed with RNase-H-treated negative patient samples (confirmed with qRT-PCR) are shown in Fig. 5c; in addition to the two reference spikes (dark grey), three further spikes were visible and corresponded with sites for S1 (blue), S2 (green) and S3 (orange). As shown above, the nanobait current signature was not affected by the complex background or unspecific binding of DNA guide oligos. The missing spike associated with specific displacement was apparent when the nanobait was mixed with the SARS-CoV-2-positive swab samples, as confirmed by qRT-PCR (Fig. 5d). We repeated the procedure for a total of 13 SARS-CoV-2 clinical samples, which contained three positive and ten negative samples (as shown by qRT-PCR). The nanobait displacement efficiencies for negative and positive samples were consistent with the qRT-PCR results (Fig. 5e).

We additionally exploited a DNA flower as an alternative to monovalent streptavidin using patient samples processed with RNase H cutting, too. We observed comparable results with this DNA-based system (Supplementary Section 13), indicating that the detection system can be based only on DNA. An all-DNA nanobait system may aid future upscaling.

Our nanobait approach bypasses preamplification and purification and hence avoids these potentially time-consuming and expensive steps. Furthermore, the nanopore readout time can be further reduced by performing a real-time analysis on the QuipuNet convolutional neural network[27]. QuipuNet has high accuracy with an analysis speed of 1,600 events per second, which is more than sufficient for rapid viral detection. In this paper, we employed standard RNA extraction procedures for the qRT-PCR tests. The speed of the test might be further improved by using simplified RNA extraction protocols or by combining it with RNase H cutting[28,29].

Conclusions

Here we demonstrate the site-specific excision of a target from long viral RNA using RNase H cutting. In this way, we increase the displacement efficiency by ensuring the exact target sequence for displacement reaction in comparison to non-specific RNA fragmentation[30]. RNase H can be used to cut sequences next to a target sequence that yields new functionality besides its use in amplification-based viral detection protocols[31]. Additionally, site-specific RNA cutting can be achieved using DNAzymes or even the CRISPR/Cas system[32,33].

Previous nanopore studies have demonstrated the ability to detect one or a limited number of short nucleic acid species in the isolated form[10,15,30,34–36]. However, the biological complexity within a test sample poses a specific challenge when wanting to discriminate targets in this complex background[11,37]. Our work demonstrates that DNA nanotechnology can be used to detect specific targets in clinical samples with nanopores. As a proof of concept, we tested the nanobait against five different respiratory viruses or SARS-CoV-2 variants in parallel. Previously, we showed that with DNA encoding, a library of 2^{112} molecules that ensures the potential to test for hundreds and thousands of viral targets in parallel can be created[12,38], especially when multiplexed nanopore systems become more advanced.

Recent studies have developed a viral nucleic acid detection system using nanopores, which holds great promise for a rapid detection

https://doi.org/10.1038/s41565-022-01287-x

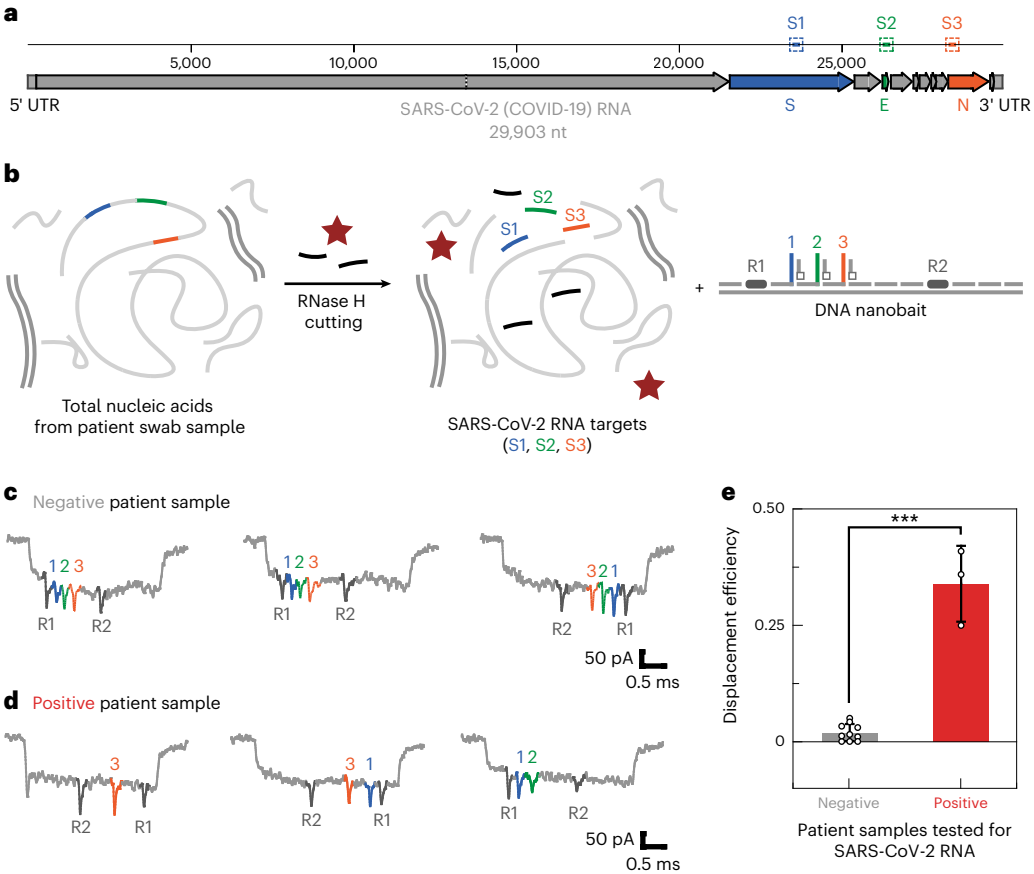

Fig. 5 | SARS-CoV-2 detection in patient's oropharyngeal swab samples. a, We designed three targets (S1, S2 and S3) in conserved regions that code for spike (S), envelope (E) and nucleocapsid (N) proteins, as indicated in the schematic of the SARS-CoV-2 RNA genome (29,903 nt long). **b**, Total nucleic acids from oropharyngeal swabs contain a mix of human DNA and RNA that either have tested positive or negative for COVID-19 with qRT-PCR. The next step included RNase H target release from long RNA and mixing with the nanobait. If targets are present, they displace the oligo harbouring a label. In this way, the displacement efficiency for each site is detectable with nanopores with 1 pM of nanobait. A real-time analysis in a mixture of various biomacromolecules (human DNA, human RNA, RNase H, streptavidin and guide oligos) is directly performed without prior purification, enabling rapid nanopore readout (~10 min). **c**,**d**, Example events for both negative (**c**) and positive (**d**) SARS-CoV-2 samples. **e**, Displacement efficiency in negative samples differs from positive samples. The error bars indicate the standard error and the centre is the mean for all the events in the first 10 min. The difference between negative and positive samples has statistical significance (***$p < 0.001$; two-sided Student's t-test). We used thirteen patient samples ($N = 13$).

system[10,15,16]. However, preamplification and enzymatic steps in preparation for nanopore detection limit the utility of such methods, although some approaches showed the potential to omit these steps[29,30,39]. Our nanobait system does not necessitate preamplification and can identify native RNA sequences without the need for sequencing. The design of this approach overcomes an issue of non-specific spikes in nanopore measurements by using the absence of a downward spike as a positive signal for the identification of the presence of the target sequence. The nanobait demonstrated comparable features to the existing methods (Supplementary Data 1)[6,40–43], and it can also identify multiple targets from the same viral RNA, thereby offering enhanced specificity and accuracy for viral identification, as demonstrated for the detection of SARS-CoV-2 in clinical specimens. Currently, we show that a 10 min nanobait readout with a nanopore would enable the detection of viral RNA in infectious patients with cycle threshold (CT) value of <20 (Fig. 5). Nanopores have single-molecule sensitivity; however, the number of events depends on the target concentration[35]. Hence, lower concentrations (CT > 20) can be measured by either a single nanopore running for a longer time or many nanopores in parallel. Here the detection time scales with $1/N$, where N is the number of nanopores.

Rapid programmability of diagnostic platforms is of paramount importance for detecting new viruses or their variants as they arise[17]. A nanobait is rapidly adaptable for new viral targets, as we demonstrated by discriminating emerging SARS-CoV-2 variants. Our study has the potential to enable amplification-free native RNA identification. The nanobait bypasses amplification sequence biases by detecting innate RNA diversity. Our results show that a nanobait can identify short and long RNAs and may find wider applications in the analysis of physiological and pathological conditions including cancer detection.

In conclusion, we have demonstrated the simultaneous identification of nucleic acids from multiple viruses and SARS-CoV-2 RNA variants in a specific and rapid manner by combining DNA nanotechnology and nanopore sensing. We employed the easily programmable nanobait with strand displacement for discrimination between SARS-CoV-2 WT RNA from variant RNA, comprising three variants of epidemiological concern[17]. Finally, we successfully used the nanobait-based nanopore-sensing method in clinical samples and could accurately determine the presence or absence of SARS-CoV-2 in patient swabs. Nanobait circumvents the need for reverse transcription, amplification, or reaction purification, and therefore bypasses enzymatic biases and some additional steps. As the nanobait has proven to be specific and accurate for viral detection in patient samples, we think our platform can be employed for native RNA detection. The nanobait paves

the way for a multiplexed amplification-free RNA detection method that is dependent only on the rapid single-molecule readout of the nanobait structure.

Online content

Any methods, additional references, Nature Portfolio reporting summaries, source data, extended data, supplementary information, acknowledgements, peer review information; details of author contributions and competing interests; and statements of data and code availability are available at https://doi.org/10.1038/s41565-022-01287-x.

References

1. Caliendo, A. M. et al. Better tests, better care: improved diagnostics for infectious diseases. *Clin. Infect. Dis.* **57**, S139–S170 (2013).
2. Burki, T. K. The economic cost of respiratory disease in the UK. *Lancet Respir. Med.* **5**, 381 (2017).
3. Leung, N. H. L. Transmissibility and transmission of respiratory viruses. *Nat. Rev. Microbiol.* **19**, 528–545 (2021).
4. Daniel, P., Bewick, T., Welham, S., Mckeever, T. M. & Lim, W. S. Adults miscoded and misdiagnosed as having pneumonia: results from the British Thoracic Society pneumonia audit. *Thorax* **72**, 376–379 (2017).
5. Methods for the detection and identification of SARS-CoV-2 variants. World Health Organization, Regional Office for Europe (2021); https://doi.org/10.1002/9781119650034.ch16
6. Esbin, M. N. et al. Overcoming the bottleneck to widespread testing: a rapid review of nucleic acid testing approaches for COVID-19 detection. *RNA* **26**, 771–783 (2020).
7. Caliendo, A. M. Multiplex PCR and emerging technologies for the detection of respiratory pathogens. *Clin. Infect. Dis.* **52**, 326–330 (2011).
8. Verschueren, D. V. et al. Label-free optical detection of DNA translocations through plasmonic nanopores. *ACS Nano* **13**, 61–70 (2019).
9. Ivankin, A. et al. Label-free optical detection of biomolecular translocation through nanopore arrays. *ACS Nano* **8**, 10774–10781 (2014).
10. Stein, U. et al. Quantification of mRNA expression using single-molecule nanopore sensing. *ACS Nano* **14**, 13964–13974 (2020).
11. Galenkamp, N. S., Soskine, M., Hermans, J., Wloka, C. & Maglia, G. Direct electrical quantification of glucose and asparagine from bodily fluids using nanopores. *Nat. Commun.* **9**, 4085 (2018).
12. Bell, N. A. W. & Keyser, U. F. Digitally encoded DNA nanostructures for multiplexed, single-molecule protein sensing with nanopores. *Nat. Nanotechnol.* **11**, 645–651 (2016).
13. Wölfel, R. et al. Virological assessment of hospitalized patients with COVID-2019. *Nature* **581**, 465–469 (2020).
14. Pan, Y., Zhang, D., Yang, P., Poon, L. L. M. & Wang, Q. Viral load of SARS-CoV-2 in clinical samples. *Lancet Infect. Dis.* **20**, 411–412 (2020).
15. Sethi, K. et al. Direct detection of conserved viral sequences and other nucleic acid motifs with solid-state nanopores. *ACS Nano* **15**, 8474–8483 (2021).
16. Beamish, E., Tabard-Cossa, V. & Godin, M. Programmable DNA nanoswitch sensing with solid-state nanopores. *ACS Sens.* **4**, 2458–2464 (2019).
17. Konings, F. et al. SARS-CoV-2 variants of interest and concern naming scheme conducive for global discourse. *Nat. Microbiol.* **6**, 821–823 (2021).
18. Fairhead, M., Krndija, D., Lowe, E. D. & Howarth, M. Plug-and-play pairing via defined divalent streptavidins. *J. Mol. Biol.* **426**, 199–214 (2014).
19. Kong, J., Zhu, J., Chen, K. & Keyser, U. F. Specific biosensing using DNA aptamers and nanopores. *Adv. Funct. Mater.* **29**, 1807555 (2019).
20. Dekker, C. Solid-state nanopores. *Nat. Nanotechnol.* **2**, 209–215 (2007).
21. Liu, H. et al. Kinetics of RNA and RNA:DNA hybrid strand displacement. *ACS Synth. Biol.* **10**, 3066–3073 (2021).
22. Rambaut, A. et al. A dynamic nomenclature proposal for SARS-CoV-2 lineages to assist genomic epidemiology. *Nat. Microbiol.* **5**, 1403–1407 (2020).
23. Kong, J., Zhu, J. & Keyser, U. F. Single molecule based SNP detection using designed DNA carriers and solid-state nanopores. *Chem. Commun.* **53**, 436–439 (2016).
24. Reynolds, A. et al. Rational siRNA design for RNA interference. *Nat. Biotechnol.* **22**, 326–330 (2004).
25. Zuker, M. & Stiegler, P. Optimal computer folding of large RNA sequences using thermodynamics and auxiliary information. *Nucleic Acids Res.* **9**, 133–148 (1981).
26. Parmar, S. et al. A blueprint for the implementation of a validated approach for the detection of SARS-Cov2 in clinical samples in academic facilities. *Wellcome Open Res.* **5**, 110 (2020).
27. Misiunas, K., Ermann, N. & Keyser, U. F. QuipuNet: convolutional neural network for single-molecule nanopore sensing. *Nano Lett.* **18**, 4040–4045 (2018).
28. Smyrlaki, I. et al. Massive and rapid COVID-19 testing is feasible by extraction-free SARS-CoV-2 RT-PCR. *Nat. Commun.* **11**, 4812 (2020).
29. Arizti-Sanz, J. et al. Simplified Cas13-based assays for the fast identification of SARS-CoV-2 and its variants. *Nat. Biomed. Eng.* **6**, 932–943 (2022).
30. Zhou, L. et al. Programmable low-cost DNA-based platform for viral RNA detection. *Sci. Adv.* **6**, eabc6246 (2020).
31. Qian, J. et al. An enhanced isothermal amplification assay for viral detection. *Nat. Commun.* **11**, 5920 (2020).
32. Wang, Y., Nguyen, K., Spitale, R. C. & Chaput, J. C. A biologically stable DNAzyme that efficiently silences gene expression in cells. *Nat. Chem.* **13**, 319–326 (2021).
33. O'Connell, M. R. et al. Programmable RNA recognition and cleavage by CRISPR/Cas9. *Nature* **516**, 263–266 (2014).
34. Cao, C. et al. Aerolysin nanopores decode digital information stored in tailored macromolecular analytes. *Sci. Adv.* **6**, eabc2661 (2020).
35. Wanunu, M. et al. Rapid electronic detection of probe-specific microRNAs using thin nanopore sensors. *Nat. Nanotechnol.* **5**, 807–814 (2010).
36. Maglia, G., Heron, A. J., Stoddart, D., Japrung, D. & Bayley, H. Analysis of single nucleic acid molecules with protein nanopores. *Methods Enzymol.* **475**, 591–623 (2010).
37. Raveendran, M., Lee, A. J., Sharma, R., Wälti, C. & Actis, P. Rational design of DNA nanostructures for single molecule biosensing. *Nat. Commun.* **11**, 4384 (2020).
38. Chen, K. et al. Digital data storage using DNA nanostructures and solid-state nanopores. *Nano Lett.* **19**, 1210–1215 (2019).
39. Kumar, N., Shetti, N. P., Jagannath, S. & Aminabhavi, T. M. Electrochemical sensors for the detection of SARS-CoV-2 virus. *Chem. Eng. J.* **430**, 132966 (2022).
40. Peinetti, A. S. et al. Direct detection of human adenovirus or SARS-CoV-2 with ability to inform infectivity using DNA aptamer-nanopore sensors. *Sci. Adv.* **7**, eabh2848 (2021).
41. Arima, A. et al. Selective detections of single-viruses using solid-state nanopores. *Sci. Rep.* **8**, 16305 (2018).
42. Taniguchi, M. et al. Combining machine learning and nanopore construction creates an artificial intelligence nanopore for coronavirus detection. *Nat. Commun.* **12**, 3726 (2021).

43. Nouri, R., Jiang, Y., Tang, Z., Lian, X. L. & Guan, W. Detection of SARS-CoV-2 with solid-state CRISPR-Cas12a-assisted nanopores. *Nano Lett.* **21**, 8393–8400 (2021).

Publisher's note Springer Nature remains neutral with regard to jurisdictional claims in published maps and institutional affiliations.

Open Access This article is licensed under a Creative Commons Attribution 4.0 International License, which permits use, sharing, adaptation, distribution and reproduction in any medium or format, as long as you give appropriate credit to the original author(s) and the source, provide a link to the Creative Commons license, and indicate if changes were made. The images or other third party material in this article are included in the article's Creative Commons license, unless indicated otherwise in a credit line to the material. If material is not included in the article's Creative Commons license and your intended use is not permitted by statutory regulation or exceeds the permitted use, you will need to obtain permission directly from the copyright holder. To view a copy of this license, visit http://creativecommons.org/licenses/by/4.0/.

© The Author(s) 2023

Methods

Patient sample collection

Patient samples were collected by swabbing the back of the throat (oropharyngeal swab) of patients, as previously described[26]. The samples were collected from patients with the COVID-19-like clinical picture and were tested with qRT-PCR after nucleic acid extraction. Briefly, after collection, swabs were placed into a labelled sample tube containing a lysis buffer (4 M guanidine thiocyanate, 25 mM Tris–HCl, 0.5% β-mercaptoethanol and MS2 RNA (200 ng μl^{-1}; Roche)). The tube was gently agitated to ensure the even distribution of lysis buffer. The safety steps have been previously described and were performed in a certified CL2 laboratory[26].

Nucleic acid extraction

The total nucleic acid was extracted using spin-column-based systems and as employed by standardized qRT-PCR testing[26]. The internal amplification control (MS2 (~6×10^4 PFU ml^{-1}) per 10 ml of lysis buffer) was added in the top-up lysis buffer (25 µl per 10 ml of lysis buffer). The sample was eluted in 100 µl of nuclease-free water (nfH_2O; Invitrogen) and left to stand for 1 min before centrifugation for 1 min at 21,130×*g* (15,000 rpm) in a benchtop microfuge. The eluted samples were directly subjected to qRT-PCR. The remaining nucleic acid extracts were stored at −80 °C and further used for nanobait–nanopore sensing.

qRT-PCR for SARS-CoV-2

SARS-CoV-2 detection was performed as previously described[26]. Per reaction, the master mix contained 12.5 µl of 2× Luna Universal Probe One-Step reaction mix, 0.5 µl of 20 µM Wu forward primer (5′-ATGGGTTGGGATTATCCTAAATGTGA-3′), 0.5 µl of 20 µM Wu reverse primer (5′-GCAGTTGTGGCATCTCCTGATGAG-3′), 0.3 µl of 10 µM MGB Probe 3 fluorescein (5′-ATGCTTAGAATTATGGCCTCAC-3′), 0.5 µl of 10 µM of internal control forward primer for MS2 RNA, 0.5 µl of 10 µM internal control reverse primer for MS2 RNA, 0.3 µl of 10 µM internal probe (MS2 ROX), 1 µl of Luna WarmStart RT Enzyme Mix and 3.9 µl of nfH_2O. Then, 20 µl of the master mix was aliquoted into each well of a 96-well plate and then combined with 5 µl of each extract. The MS2 internal extraction and amplification control that underwent the full extraction protocol was included as the negative extraction control in a minimum of two wells on the qRT-PCR plate. To determine potential contamination in the qRT-PCR process, 5 µl nfH_2O was included as the qRT-PCR negative control. Then, 5 µl of spiked SARS-CoV-2 template plasmid was included in a single well as the qRT-PCR positive control. After adding 5 µl of each sample to its designated well, the plate was sealed with an optically clear plastic seal. The plate was centrifuged for 1 min at 2,000×*g* (1,000 rpm) at 4 °C and then inserted in the qRT-PCR machine (QuantStudio, Thermo Fisher Scientific) and the run was parametrized. Signals for fluorescein (FAM) and carboxyrhodamine (ROX) were acquired. ROX was used to detect the internal MS2 control and fluorescein was used to detect SARS-CoV-2 RNA. The assay was performed for 2 min at 25 °C, 15 min at 50 °C (for the reverse transcriptase), 2 min at 90 °C, before 45 cycles of 95 °C for 3 s followed by 60 °C for 30 s. The results were determined by the confirmation of correct positive controls (amplification of the plasmid), extraction and amplification controls of all the samples (ROX channel), no amplification in the negative controls and consistent mean values of controls. SARS-CoV-2 positivity was confirmed by amplification in the fluorescein channel with an appropriate sigmoidal curve with a CT value of ≤36. The CT values of MS2 and MGB probe 3 were maintained to track the quality and reproducibility of the assay[44].

Programmable RNase H cutting for nanobait

For nanopore sensing, SARS-CoV-2 RNA controls, nucleic acid extracts (patient samples) or MS2 viral RNA were used further for detection with nanobait. First, we mixed guide oligos with the sample and heated it to 70 °C for 5 min. RNase H (5,000 units per ml; NEB) was added, mixed and heated for 20 min at 37 °C to allow the enzyme to cut RNA in the DNA: RNA hybrid that effectively releases the target RNA. RNase H was thermally inactivated by incubation at 65 °C for 10 min. Guide oligos were validated to not form intramolecular structures, homo- or heterodimers using the NUPACK software[45]. For the measurement with the absent target, the same protocol including guide oligos was used. The control measurements show no displacement, and hence, we can exclude any substantial cross-binding from guide oligos.

Viral target sequence properties for nanobait

The length of target, toehold length and GC content were selected to ensure optimal hybridization[21]. For the DNA nanobait designs, the target sequences were selected to be in the conserved regions of a viral genome and had 40–60% GC content to form a stable 20 bp duplex. The toehold length was selected to be 6 nt long and have 40–60% GC content. We tested all the sequences for potential undesirable highly stable intramolecular interactions or homodimers using the NUPACK software (web application 2020)[45]. Then, we performed a cross-reactivity check between multiple sites employed in each experiment[45].

Preparation of DNA flower for nanobait

We designed a DNA flower as another label for SARS-CoV-2 RNA detection from the patient samples. Three DNA flowers specific for each SARS-CoV-2 target (seven-way junctions, 7WJa, 7WJb and 7WJc) were separately prepared. Taking 7WJc as an example, 4 µM DNA strand J1, J2, J3 and J4c (Supplementary Table 1) were mixed together in TM buffer (10 mM Tris–HCl, 10 mM $MgCl_2$, pH 8.0) and heated to 90 °C for 5 min, then cooled down to 65 °C for 15 min, 45 °C for 15 min, 37 °C for 20 min, 25 °C for 20 min and finally to 4 °C for 20 min. Strand J4c was substituted by J4b to prepare 7WJb. For 7WJa, to avoid self-folding at site 43 on the nanobait, J1, J2, J3 J4a and C43 were mixed together before annealing.

Self-assembly of DNA nanobait

The DNA nanobait was assembled by mixing linearized single-stranded M13 DNA (M13mp18, 7,249 nt, Guild Biosciences, 100 nM) with short complementary oligonucleotides[12] (some of which harboured reference structures and capture strands) and by adding partially complementary strands that were 3′-biotinylated for toehold-mediated strand displacement reaction. The linearized M13 DNA (7,228 nt in length) was complemented by oligonucleotides, thereby creating a nicked double-stranded nanobait with two-terminal four deoxythymidine overhangs that prevent multimerization[12]. The mix contained 20 nM of linearized M13 DNA, 60 nM of oligonucleotides (three times excess to M13 DNA), 3′-biotinylated strands in the concentration of 180 nM, 10 mM $MgCl_2$ and 1× TE (10 mM Tris–HCl, 1 mM EDTA, pH 8.0). It was mixed by pipetting and spun down before heating to 70 °C for 30 s and cooled down over 45 min to ambient temperature. Excess oligonucleotides were removed using Amicon Ultra 0.5 ml centrifugal filters with 100 kDa cutoff with a washing buffer (10.0 mM Tris–HCl pH 8.0, 0.5 mM $MgCl_2$). If DNA flowers were employed as a label, the partially complementary strands that carry it were incubated in 10 mM $MgCl_2$ for 2 h at ambient temperature, and subsequently, Amicon filtration was performed as described above. The asymmetry of the nanobait design allows for the unambiguous identification of the binding sites. The nanobait was stored until used for further experiments under 4–10 °C in 0.5 mM $MgCl_2$, 10.0 mM Tris–HCl, pH 8.0. The nanobait design was checked by nanopore readout before each measurement.

Nanopore readout of DNA nanobait

The nanobait was mixed with a sample (nucleic acid extract or purified viral targets at ten times excess) in 10 mM $MgCl_2$ and 100 mM NaCl.

The mixture (5 µl) was incubated at room temperature (~10 min) until prepared for nanopore measurement. The difference in the target sequence composition and its physical characteristics might lead to variability in hybridization and hence the displacement efficiency of sensing sites[21]. We have used htRNA (100 ng µl^{-1}; Invitrogen) as a background where indicated, to show that there are no non-specific signals induced by human native RNAs. For nanopore measurement, the sample was diluted to <0.5 nM nanobait (for purified viral targets) or 4.7 µl of RNase-H-cut patient sample was mixed with 0.3 µl of monovalent streptavidin (SAe1D3)[18] (1 µM), 5 µl of LiCl (4.0 M) and 5.0 µl of LiCl (8.0 M). We have fabricated 14 ± 3 nm (mean ± standard deviation) nanopores[12] using quartz glass capillaries with 0.5 mm outer diameter and 0.2 mm inner diameter (Sutter Instrument) by laser-assisted puller P-2000 (Sutter Instrument). The mix was pipetted in a nanopore polydimethylsiloxane chip, and all the measurements were performed at a constant voltage of 600 mV. Nanopore measurement details are shown in Supplementary Table 30.

Real-time nanopore data analysis

Nanopore data analysis is explained in detail in Supplementary Section 14. Briefly, nanobait events were filtered out of raw ionic current traces and then the detection region was determined, and information of the spike's presence at each specific site was extracted. The plotted displacement efficiency was calculated as a displacement efficiency for a measurement subtracted to a no-target control for each site (50 nanobait events for each of the three nanopore recordings), unless stated otherwise:

$$\text{Displacement efficiency} = \frac{1}{3}\sum_{n=1}^{3}\left\{1-\frac{1}{50}\sum_{n=1}^{50}\left[f(n)=\left(\frac{1,\text{peak}}{0,\text{no peak}}\right)\right]_{\text{target}}\right\} - \frac{1}{3}\sum_{n=1}^{3}\left\{1-\frac{1}{50}\sum_{n=1}^{50}\left[f(n)=\left(\frac{1,\text{peak}}{0,\text{no peak}}\right)\right]_{\text{no target}}\right\}$$

We verified that the convolutional neural network QuipuNet[27] was capable of the real-time analysis of nanopore data following the described procedure. Previously, we demonstrated that with around ten events, we reach 99% confidence in a positive detection of our designed DNA structures[46].

AFM imaging

AFM (Nanosurf Mobile S) imaging of nanobaits was performed in air in the non-contact mode. The nanobait structures were diluted to 1 ng µl^{-1} in 1 mM $MgCl_2$ and 10 µl was added to freshly cleaved mica, incubated for 1 min, rinsed with filtered Milli-Q water and then blow dried with nitrogen. Before scanning, the mica plate was affixed to the AFM sample stage using double-sided adhesive tape. Image visualization and analysis were performed using Gwyddion (version 2.60).

Statistical analysis

For all the measurements, 99.9% confidence intervals for displacement efficiencies were calculated. Statistical significance between two sites without and with the target was tested using a two-sided Student's *t*-test.

Reporting summary

Further information on research design is available in the Nature Portfolio Reporting Summary linked to this article.

Data availability

Data supporting the findings of this study are available in the main text and Supplementary Information. Additional raw data are available at https://doi.org/10.17863/CAM.89753. Source data are provided with this paper.

References

44. Westgard, J. O., Groth, T., Aronsson, T., Falk, H. & de Verdier, C. H. Performance characteristics of rules for internal quality control: probabilities for false rejection and error detection. *Clin. Chem.* **23**, 1857–1867 (1977).
45. Wolfe, B. R., Porubsky, N. J., Zadeh, J. N., Dirks, R. M. & Pierce, N. A. Constrained multistate sequence design for nucleic acid reaction pathway engineering. *J. Am. Chem. Soc.* **139**, 3134–3144 (2017).
46. Zhu, J., Ermann, N., Chen, K. & Keyser, U. F. Image encoding using multi-level DNA barcodes with nanopore readout. *Small* **17**, 2100711 (2021).

Acknowledgements

We thank P. Lehner for his evaluation of the project and advice on unmet diagnostic needs and N. Bell for help with the AFM imaging of DNA structures. We thank T. Fitzmaurice for his operational help during the COVID-19 pandemic. We acknowledge the Statistics Clinic, Centre for Mathematical Sciences, for their guidelines on a statistical analysis of the data presented in this study. Funding: J.Z., K.C. and U.F.K. acknowledge funding from a European Research Council (ERC) consolidator grant (DesignerPores no. 647144). U.F.K., S.B. and J.Z. were supported by a Wellcome Trust DCF grant. K.C. and U.F.K. acknowledge support through an ERC-2019-PoC grant (PoreDetect no. 899538). F.B. acknowledges funding from the George and Lilian Schiff Foundation Studentship, the Winton Programme for the Physics of Sustainability PhD Scholarship and St John's College Benefactors' Scholarship. A.O. acknowledges funding from the Cambridge Trust Vice Chancellor's Award. R.T. acknowledges funding from the European Union's Horizon 2020 research and innovation programme under the Marie Skłodowska-Curie grant agreement no. 892333, and from the Blavatnik Family Foundation. M.F.A. acknowledges funding from UKSCAB scholarship. N.E. acknowledges funding from the EPSRC, Cambridge Trust, and Trinity Hall, Cambridge. M.F. and M.H. acknowledge funding from the Biotechnology and Biological Sciences Research Council (BBSRC, BB/I006303/1). This work was supported by the NIHR Cambridge Biomedical Research Centre and NIHR AMR Research Capital Funding Scheme (NIHR200640). The views expressed are those of the author(s) and not necessarily those of the NIHR or the Department of Health and Social Care. S.B. is supported by a Wellcome Trust senior research fellowship (215515/Z/19/Z). The funders had no role in study design, data collection and analysis, decision to publish or preparation of the manuscript.

Author contributions

F.B. and U.F.K. conceived the idea. F.B., J.Z., K.C. and M.F.A. prepared the nanobait designs. J.Z. and F.B. designed the sequences for the respective targets. F.B. performed the experiments using monovalent streptavidin. J.Z. performed the experiments using DNA flower and assembled the DNA flower. A.O. and F.B. performed the gel electrophoresis and analysed the corresponding data. F.B. performed the electrophoretic mobility shift assay. R.T. performed the AFM imaging of the nanobait. F.B., J.Z. and M.Đ. analysed the nanopore data. J.P.D. and S.B. collected the oropharyngeal patient samples, extracted the nucleic acids and performed qRT-PCR. M.F. and M.H. prepared the monovalent streptavidin. F.B. and U.F.K. wrote the initial manuscript draft. F.B., J.Z., A.O. and K.C. prepared the draft manuscript. All authors contributed to the discussion and final manuscript version.

Competing interests

F.B. and U.F.K. are inventors of the nanobait method (UK Patent application nos. 2112088.6 and PCT/GB2022/052171, in process) submitted by Cambridge Enterprise on the behalf of the University of Cambridge. U.F.K., K.C. and M.A. are co-founders of Cambridge Nucleomics. All other authors have no competing interests.

Additional information

Supplementary information The online version contains supplementary material available at https://doi.org/10.1038/s41565-022-01287-x.

Correspondence and requests for materials should be addressed to Ulrich F. Keyser.

Peer review information *Nature Nanotechnology* thanks Cesar de la Fuente, Meni Wanunu and the other, anonymous, reviewer(s) for their contribution to the peer review of this work.

Reprints and permissions information is available at www.nature.com/reprints.

nature portfolio

Corresponding author(s): Ulrich F. Keyser

Last updated by author(s): Oct 20, 2022

Reporting Summary

Nature Portfolio wishes to improve the reproducibility of the work that we publish. This form provides structure for consistency and transparency in reporting. For further information on Nature Portfolio policies, see our Editorial Policies and the Editorial Policy Checklist.

Statistics

For all statistical analyses, confirm that the following items are present in the figure legend, table legend, main text, or Methods section.

n/a	Confirmed	
☐	☒	The exact sample size (*n*) for each experimental group/condition, given as a discrete number and unit of measurement
☐	☒	A statement on whether measurements were taken from distinct samples or whether the same sample was measured repeatedly
☐	☒	The statistical test(s) used AND whether they are one- or two-sided *Only common tests should be described solely by name; describe more complex techniques in the Methods section.*
☒	☐	A description of all covariates tested
☒	☐	A description of any assumptions or corrections, such as tests of normality and adjustment for multiple comparisons
☐	☒	A full description of the statistical parameters including central tendency (e.g. means) or other basic estimates (e.g. regression coefficient) AND variation (e.g. standard deviation) or associated estimates of uncertainty (e.g. confidence intervals)
☐	☒	For null hypothesis testing, the test statistic (e.g. *F*, *t*, *r*) with confidence intervals, effect sizes, degrees of freedom and *P* value noted *Give P values as exact values whenever suitable.*
☒	☐	For Bayesian analysis, information on the choice of priors and Markov chain Monte Carlo settings
☒	☐	For hierarchical and complex designs, identification of the appropriate level for tests and full reporting of outcomes
☒	☐	Estimates of effect sizes (e.g. Cohen's *d*, Pearson's *r*), indicating how they were calculated

Our web collection on statistics for biologists contains articles on many of the points above.

Software and code

Policy information about availability of computer code

Data collection	The data was collected using software written with LabView 2013 (National Instruments). Nupack online (http://www.nupack.org/).
Data analysis	Data analysis was also performed using software written with LabView 2013 (National Instruments).

For manuscripts utilizing custom algorithms or software that are central to the research but not yet described in published literature, software must be made available to editors and reviewers. We strongly encourage code deposition in a community repository (e.g. GitHub). See the Nature Portfolio guidelines for submitting code & software for further information.

Data

Policy information about availability of data

All manuscripts must include a data availability statement. This statement should provide the following information, where applicable:

- Accession codes, unique identifiers, or web links for publicly available datasets
- A description of any restrictions on data availability
- For clinical datasets or third party data, please ensure that the statement adheres to our policy

Raw data of ionic current values for translocations together with a table summarizing all the nanopores used is available at the supplementary information and source data are available online via the repository. SARS-CoV-2 detection in clinical samples and tested with RT-qPCR are available here https://wellcomeopenresearch.org/articles/5-110/v2. Our data can be analysed with any software that allows for peak detection and even more importantly by hand.

Field-specific reporting

Please select the one below that is the best fit for your research. If you are not sure, read the appropriate sections before making your selection.

☒ Life sciences ☐ Behavioural & social sciences ☐ Ecological, evolutionary & environmental sciences

For a reference copy of the document with all sections, see nature.com/documents/nr-reporting-summary-flat.pdf

Life sciences study design

All studies must disclose on these points even when the disclosure is negative.

Sample size	We have measured on each nanopore device as long as the device are usable. Briefly, nanobait events were filtered out of raw ionic current traces, then the detection region was determined, and information of the spike's presence at each specific site was extracted. The displacement efficiency was calculated as a difference between a no target control and a measurement for each site. We measured during the lifetime of nanopore and first fifty nanobait events for each of three nanopore recordings were further used for analysis. 99.9% confidence intervals for the displacement efficiencies were calculated for all measurements. The statistical significance between two sites without and with the target was tested using a student's T-test.
Data exclusions	Our data analysis exclude fragments of DNA, cut RNA, proteins as well as aggregates that are excluded based on event charge deficit of nanopore event and the absence of reference structures.
Replication	The measurements presented in the main text were repeated using at least three different nanopores and experiments. These results are presented in the supplementary information. Each repeat successfully confirmed the central findings.
Randomization	Randomization was not relevant to this study since we were not comparing experimental groups rather demonstrating method applicability.
Blinding	Blinding was not relevant to this study since we were not comparing experimental groups. We did blind study for the patient samples analysis.

Reporting for specific materials, systems and methods

We require information from authors about some types of materials, experimental systems and methods used in many studies. Here, indicate whether each material, system or method listed is relevant to your study. If you are not sure if a list item applies to your research, read the appropriate section before selecting a response.

Materials & experimental systems

n/a	Involved in the study
☒	☐ Antibodies
☒	☐ Eukaryotic cell lines
☒	☐ Palaeontology and archaeology
☒	☐ Animals and other organisms
☒	☐ Human research participants
☒	☐ Clinical data
☒	☐ Dual use research of concern

Methods

n/a	Involved in the study
☒	☐ ChIP-seq
☒	☐ Flow cytometry
☒	☐ MRI-based neuroimaging

nature nanotechnology

Article

https://doi.org/10.1038/s41565-022-01287-x

Simultaneous identification of viruses and viral variants with programmable DNA nanobait

In the format provided by the authors and unedited

Supplementary Information

Simultaneous identification of viruses and viral variants with programmable DNA nanobait

Filip Bošković[1], Jinbo Zhu[1], Ran Tivony[1], Alexander Ohmann [1], Kaikai Chen[1], Mohammed F. Alawami[1], Milan Đorđević [1], Niklas Ermann[1], Joana Pereira Dias[2,3], Michael Fairhead[4], Mark Howarth[4], Stephen Baker[2,3], Ulrich F. Keyser[1,*]

[1] Cavendish Laboratory, University of Cambridge, JJ Thomson Avenue, Cambridge, CB3 0HE, UK

[2] University of Cambridge School of Clinical Medicine, Cambridge Biomedical Campus, Hills Road, Cambridge, CB2 0SP, UK

[3] Department of Medicine, University of Cambridge School of Clinical Medicine, Cambridge Biomedical Campus, Hills Road, Cambridge, CB2 0QQ, UK

[4] Department of Biochemistry, University of Oxford, South Parks Road, Oxford, OX1 3QU, UK

[*] *corresponding author*

This file includes:

Table of Contents

Section S1. DNA nanobait

Section S1.1 Nanobait design

Nanobait is assembled by mixing the linearized DNA scaffold (M13mp18, 7228 nt, Guild Biosciences, 100 nM) with short complementary oligos[1]. The basic set of oligos has 188 oligos which are 38 nt long and two terminal oligos that are 46 nt long (with four terminal T to avoid aggregation by blunt-end stacking[1–3]) that are complementary to the 7228 nt long scaffold. These oligos are provided in Table S2. Certain oligos from Table S2 were replaced with oligos that code references (listed in Table S3) and capture oligos that are specific for five targets. Nanobait has a detection region that is marked by two references and contains five capture strands specific to five targets (Figure S1a).

Each reference has six interspaced DNA dumbbells (schematic design is shown in Figure S1b) i.e. DNA double hairpins (5'-TCCTCTTTTGAGGAACAAGTTTTCTTGT-3') that are interpreted as one downward signal in nanopore events due to their close proximity[4,5]. In addition to the capturing oligo (which contains two regions, one comprising 38 nt complementary to the DNA scaffold and one comprising 20 nt complementary to the target), each capture site contains a partially complementary oligo (14 nt) that carries a label (Figure S1c). This single-stranded region of the capture strand contains a toehold (6 nt) needed for strand displacement reaction (SDR). Once a target is added to the solution, it first binds to the toehold and then it's able to displace the oligo with a label (Figure S1d). Hence, target presence is detected as the absence of oligo with a label (which is read as a missing peak in nanopore event).

Section S1.2 Linearization of circular single-stranded M13

Linearization of circular M13 scaffold (M13mp18, 7249 nt) is performed using double restriction digestion. Firstly, we bound an oligonucleotide (39 nt long, 5'-TCTAGAGGATCCCCGGGTACCGAGCTCGAATTCGTAATC-3') to the scaffold to create a double-stranded region for efficient enzyme digestion. Such a double-stranded region contains closely spaced restriction sites for EcoRI and BamHI enzymes. The double enzyme digestion is used to ensure complete linearization of the scaffold. We mixed 52 µL of scaffold (M13mp18, 100 nM) with 10 µL of 10 × CutSmart buffer (1 × buffer components are 50 mM potassium acetate, 20 mM Tris-acetate, 10 mM magnesium acetate, 100 µg/ml BSA, pH 7.9 at 25 °C; New England Biolabs), 2.5 µL of 39 nt long oligo (100 µM in H_20, IDT), and 33.5 µL of filtered Milli-Q water. The mix was heated to 65 °C for 30 s and slowly cooled down to 25 °C over ~40 min. After oligo

binding, 1 µL of EcoRI-HF enzyme (100,000 units/mL) and1 µL of BamHI-HF enzyme (100,000 units/mL) was added to the reaction and mixed by pipetting the full volume multiple times and incubated at 37 °C for 1 h. The cut scaffold was purified as previously described using NucleoSpin Gel and PCR Clean-up kit (Macherey-Nagel™)[1].

Section S1.3 Nanobait assembly

Nanobait is assembled by mixing the scaffold with a respective set of oligos. Briefly, we mixed 800 fmoles of the linearized scaffold with three times excess of oligos (2400 fmoles each) in 10 mM $MgCl_2$, 1 × Tris-HCl, pH 8.0. The reaction was heated to 70 °C for 30 s followed by linear cooling to 25 °C over 45 min. The excess oligos were removed with Amicon 0.5 mL filters with 100 kDa cut-off using a washing buffer (10 mM Tris-HCl, pH 8.0, 0.5 mM $MgCl_2$). The samples were centrifuged at 9,200 × g for 10 min twice, and after the filter was inverted, placed in a new tube, and spun down at 1,000 × g for 2 min. Nanobait concentration was estimated from a NanoDrop spectrophotometer or a Qubit fluorometer using Qubit™ dsDNA BR Assay Kit.

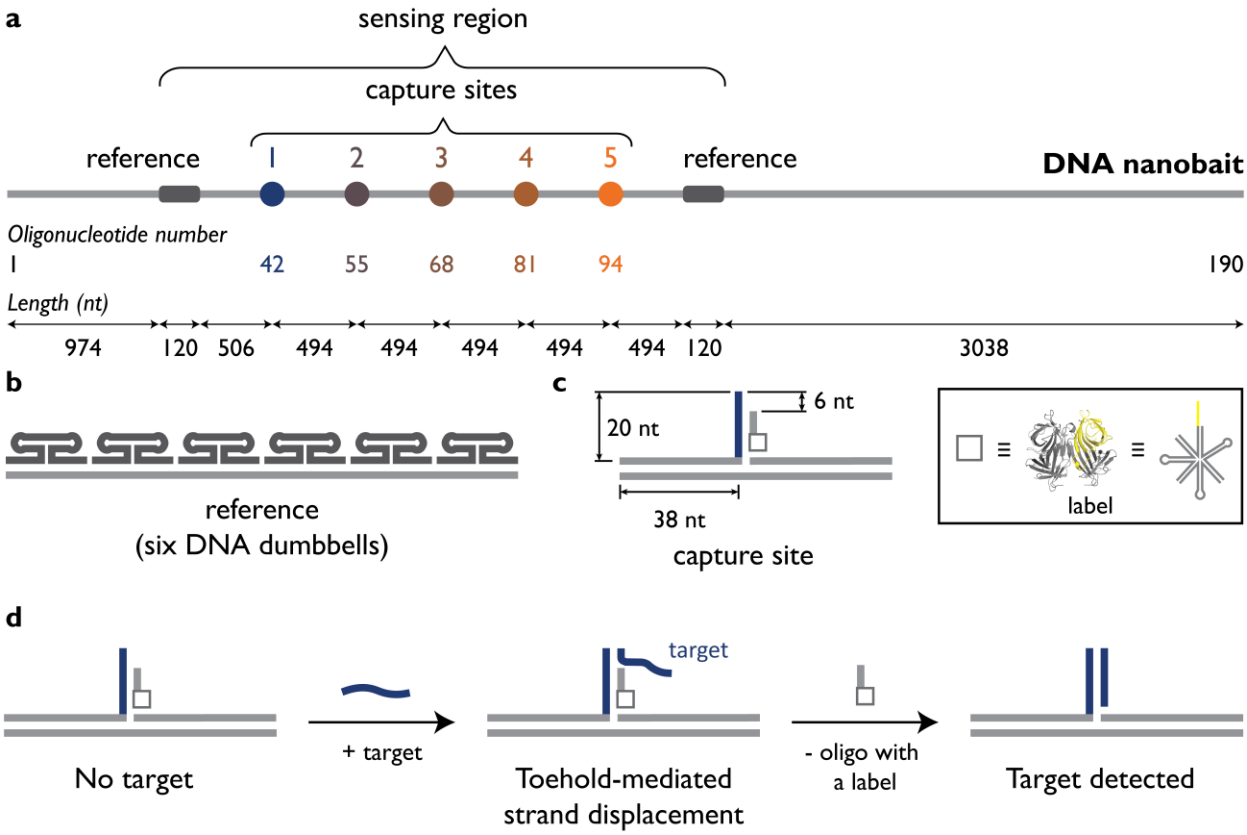

Figure S1. DNA nanobait schematic design. a) Nanobait contains a detection region that has two references (dark gray) and five capture sites for each target strand. Nanobait represents M13 DNA that is fully covered by oligonucleotides forming a double-stranded DNA with nicks. A standard set of 190

oligonucleotides was used and some of the oligonucleotides were replaced with a reference or capture strands. Oligo numbers replaced for each capture site is depicted below the nanobait. Lengths and distances between features on nanobait are represented as a number of nucleotides i.e. basepairs once a double-stranded molecule is formed. b) Reference contains six interspaced DNA dumbbells which are read as one downward signal in nanopore measurements. c) Capture site structure is represented by capture strand that has a 38 nt part complementary to the DNA scaffold and a 20 nt part that is fully complementary to a target strand. The oligo carrying the label is partially complementary to the capture strand (14 nt). The label can be either monovalent streptavidin or a DNA flower. d) The uncomplemented part of the capture strand (6 nt) is called the toehold and it serves as a seed for displacement (removal) of the oligo with a label by the target.

Section S2. Design of structural labels used for nanopore signal amplification

Specific identification of the presence or absence of the target sequence in solution is done by using nanopore sensing. In nanopore recordings, the "control" or absence of a target is detected as a downward signal or peak on a DNA event. This peak corresponds to a label that is attached to an oligonucleotide (oligo or strand) (further explained in Section S3). In this study, we demonstrated that both protein-based and DNA-based structures can be employed as labels.

As a protein-based label, we employed monovalent streptavidin (structure shown in Figure S2a) that has a single femtomolar affinity biotin binding site. Monovalent streptavidin expression and purification have been described previously[6]. Oligos have a biotin label on the 3' end via a C6 spacer arm (Integrated DNA Technologies) to which monovalent streptavidin binds.

As a DNA-based label, we assembled a DNA flower[7] that represents a 7-way junction as is illustrated in Figure S2b using four DNA strands as described in the next section. One of the strands (J4, Table S1) has 14 nt single-stranded part (in yellow) that is used as an anchor that binds to nanobait (further explained in Section S3).

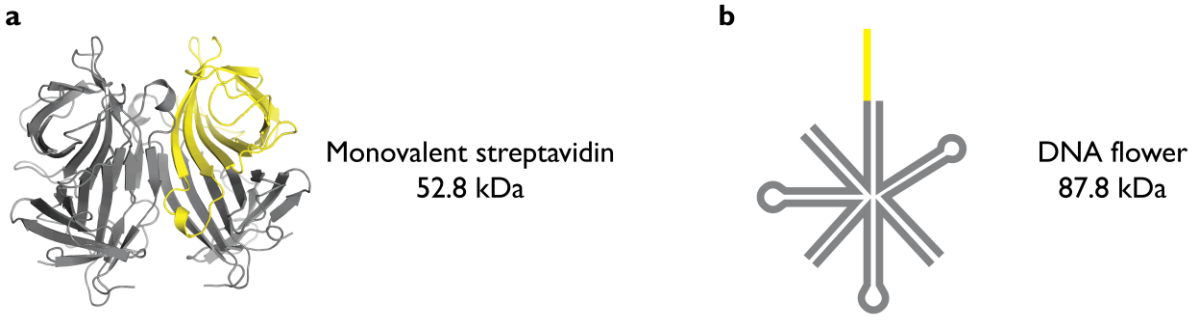

Figure S2. The designs of structures used in this study as labels. a) The tetramer is formed from one biotin-binding subunit in yellow and 3 non-binding subunits in gray (PDB ID: 5TO2). b) DNA flower represents a 7-way junction, designed with an arm length of 16 bp and loops with 4 T (gray). The region of oligo that binds to a respective site on the nanobait is in yellow.

Section S3. DNA flower synthesis

Three DNA flowers specific for each SARS-CoV-2 target (7-way junctions, 7WJa, 7WJb, and 7WJc) were prepared separately. Taking 7WJc as an example, 4 μM DNA strands J1, J2, J3,

and J4c (Table S1) were mixed in TM buffer (10 mM Tris-HCl, 10 mM $MgCl_2$, pH 8.0) and heated at 90 °C for 5 min, then cooled down to 65 °C for 15 min, 45 °C for 15 min, 37 °C for 20 min, 25 °C for 20 min and finally 4 °C for 20 min. Strand J4c was substituted by J4b to prepare 7WJb. For 7WJa, to avoid self-folding and improve the occupied fraction at site 43 on nanobait, J1, J2, J3 J4a, and C43 were mixed before annealing.

Supplementary Table S1. DNA flower oligonucleotides. The complementary parts are highlighted by using the same color.

Strand name	Sequence (5'→'3')
J1	GGATCAGAGCTGGACG ACAATGACGTAGGTCC TTTT GGACCTACGTCATTGT ACTATGGCACACATCC
J2	GCAAGACTCGTGCTCA CCGAATGCCACCACGC TTTT GCGTGGTGGCATTCGG CGTCCAGCTCTGATCC
J3	GGTTCAGCCGCAATCC TCGCCTGCACTCTACC TTTT GGTAGAGTGCAGGCGA TGAGCACGAGTCTTGC
J4a	TACTGCGCTTCGAT TT GGATGTGTGCCATAGT GGATTGCGGCTGAACC
J4b	AACTGAGGGAGCCT TT GGATGTGTGCCATAGT GGATTGCGGCTGAACC
J4c	AGACTAATTCTCCT TT GGATGTGTGCCATAGT GGATTGCGGCTGAACC

Supplementary Table S2. DNA scaffold complementary oligonucleotides

Oligo number	Sequence (5'→'3')
1	TTTTCGTAATCATGGTCATAGCTGTTTCCTGTGTGAAATTGTTATC
2	CGCTCACAATTCCACACAACATACGAGCCGGAAGCATA
3	AAGTGTAAAGCCTGGGGTGCCTAATGAGTGAGCTAACT
4	CACATTAATTGCGTTGCGCTCACTGCCCGCTTTCCAGT
5	CGGGAAACCTGTCGTGCCAGCTGCATTAATGAATCGGC
6	CAACGCGCGGGGAGAGGCGGTTTGCGTATTGGGCGCCA
7	GGGTGGTTTTTCTTTTCACCAGTGAGACGGGCAACAGC
8	TGATTGCCCTTCACCGCCTGGCCCTGAGAGAGTTGCAG
9	CAAGCGGTCCACGCTGGTTTGCCCCAGCAGGCGAAAAT
10	CCTGTTTGATGGTGGTTCCGAAATCGGCAAAATCCCTT
11	ATAAATCAAAAGAATAGCCCGAGATAGGGTTGAGTGTT
12	GTTCCAGTTTGGAACAAGAGTCCACTATTAAAGAACGT
13	GGACTCCAACGTCAAAGGGCGAAAAACCGTCTATCAGG
14	GCGATGGCCCACTACGTGAACCATCACCCAAATCAAGT
15	TTTTTGGGGTCGAGGTGCCGTAAAGCACTAAATCGGAA
16	CCCTAAAGGGAGCCCCCGATTTAGAGCTTGACGGGGAA
17	AGCCGGCGAACGTGGCGAGAAAGGAAGGGAAGAAAGCG
18	AAAGGAGCGGGCGCTAGGGCGCTGGCAAGTGTAGCGGT
19	CACGCTGCGCGTAACCACCACACCCGCCGCGCTTAATG
20	CGCCGCTACAGGGCGCGTACTATGGTTGCTTTGACGAG
21	CACGTATAACGTGCTTTCCTCGTTAGAATCAGAGCGGG
22	AGCTAAACAGGAGGCCGATTAAAGGGATTTTAGACAGG
23	AACGGTACGCCAGAATCCTGAGAAGTGTTTTTATAATC
24	AGTGAGGCCACCGAGTAAAAGAGTCTGTCCATCACGCA
25	AATTAACCGTTGTAGCAATACTTCTTTGATTAGTAATA
26	ACATCACTTGCCTGAGTAGAAGAACTCAAACTATCGGC
27	CTTGCTGGTAATATCCAGAACAATATTACCGCCAGCCA
28	TTGCAACAGGAAAAACGCTCATGGAAATACCTACATTT
29	TGACGCTCAATCGTCTGAAATGGATTATTTACATTGGC
30	AGATTCACCAGTCACACGACCAGTAATAAAAGGGACAT
31	TCTGGCCAACAGAGATAGAACCCTTCTGACCTGAAAGC
32	GTAAGAATACGTGGCACAGACAATATTTTTGAATGGCT
33	ATTAGTCTTTAATGCGCGAACTGATAGCCCTAAAACAT
34	CGCCATTAAAAATACCGAACGAACCACCAGCAGAAGAT
35	AAAACAGAGGTGAGGCGGTCAGTATTAACACCGCCTGC
36	AACAGTGCCACGCTGAGAGCCAGCAGCAAATGAAAAAT
37	CTAAAGCATCACCTTGCTGAACCTCAAATATCAAACCC
38	TCAATCAATATCTGGTCAGTTGGCAAATCAACAGTTGA
39	AAGGAATTGAGGAAGGTTATCTAAAATATCTTTAGGAG
40	CACTAACAACTAATAGATTAGAGCCGTCAATAGATAAT
41	ACATTTGAGGATTTAGAAGTATTAGACTTTACAAACAA
42	TTCGACAACTCGTATTAAATCCTTTGCCCGAACGTTAT
43	TAATTTTAAAAGTTTGAGTAACATTATCATTTTGCGGA

44	ACAAAGAAACCACCAGAAGGAGCGGAATTATCATCATA
45	TTCCTGATTATCAGATGATGGCAATTCATCAATATAAT
46	CCTGATTGTTTGGATTATACTTCTGAATAATGGAAGGG
47	TTAGAACCTACCATATCAAAATTATTTGCACGTAAAAC
48	AGAAATAAAGAAATTGCGTAGATTTTCAGGTTTAACGT
49	CAGATGAATATACAGTAACAGTACCTTTTACATCGGGA
50	GAAACAATAACGGATTCGCCTGATTGCTTTGAATACCA
51	AGTTACAAAATCGCGCAGAGGCGAATTATTCATTTCAA
52	TTACCTGAGCAAAAGAAGATGATGAAACAAACATCAAG
53	AAAACAAAATTAATTACATTTAACAATTTCATTTGAAT
54	TACCTTTTTTAATGGAAACAGTACATAAATCAATATAT
55	GTGAGTGAATAACCTTGCTTCTGTAAATCGTCGCTATT
56	AATTAATTTTCCCTTAGAATCCTTGAAAACATAGCGAT
57	AGCTTAGATTAAGACGCTGAGAAGAGTCAATAGTGAAT
58	TTATCAAAATCATAGGTCTGAGAGACTACCTTTTTAAC
59	CTCCGGCTTAGGTTGGGTTATATAACTATATGTAAATG
60	CTGATGCAAATCCAATCGCAAGACAAAGAACGCGAGAA
61	AACTTTTTCAAATATATTTTAGTTAATTTCATCTTCTG
62	ACCTAAATTTAATGGTTTGAAATACCGACCGTGTGATA
63	AATAAGGCGTTAAATAAGAATAAACACCGGAATCATAA
64	TTACTAGAAAAAGCCTGTTTAGTATCATATGCGTTATA
65	CAAATTCTTACCAGTATAAAGCCAACGCTCAACAGTAG
66	GGCTTAATTGAGAATCGCCATATTTAACAACGCCAACA
67	TGTAATTTAGGCAGAGGCATTTTCGAGCCAGTAATAAG
68	AGAATATAAAGTACCGACAAAAGGTAAAGTAATTCTGT
69	CCAGACGACGACAATAAACAACATGTTCAGCTAATGCA
70	GAACGCGCCTGTTTATCAACAATAGATAAGTCCTGAAC
71	AAGAAAAATAATATCCCATCCTAATTTACGAGCATGTA
72	GAAACCAATCAATAATCGGCTGTCTTTCCTTATCATTC
73	CAAGAACGGGTATTAAACCAAGTACCGCACTCATCGAG
74	AACAAGCAAGCCGTTTTTATTTTCATCGTAGGAATCAT
75	TACCGCGCCCAATAGCAAGCAAATCAGATATAGAAGGC
76	TTATCCGGTATTCTAAGAACGCGAGGCGTTTTAGCGAA
77	CCTCCCGACTTGCGGGAGGTTTTGAAGCCTTAAATCAA
78	GATTAGTTGCTATTTTGCACCCAGCTACAATTTTATCC
79	TGAATCTTACCAACGCTAACGAGCGTCTTTCCAGAGCC
80	TAATTTGCCAGTTACAAAATAAACAGCCATATTATTTA
81	TCCCAATCCAAATAAGAAACGATTTTTTGTTTAACGTC
82	AAAAATGAAAATAGCAGCCTTTACAGAGAGAATAACAT
83	AAAAACAGGGAAGCGCATTAGACGGGAGAATTAACTGA
84	ACACCCTGAACAAAGTCAGAGGGTAATTGAGCGCTAAT
85	ATCAGAGAGATAACCCACAAGAATTGAGTTAAGCCCAA
86	TAATAAGAGCAAGAAACAATGAAATAGCAATAGCTATC
87	TTACCGAAGCCCTTTTTAAGAAAAGTAAGCAGATAGCC
88	GAACAAAGTTACCAGAAGGAAACCGAGGAAACGCAATA
89	ATAACGGAATACCCAAAAGAACTGGCATGATTAAGACT
90	CCTTATTACGCAGTATGTTAGCAAACGTAGAAAATACA

91	TACATAAAGGTGGCAACATATAAAAGAAACGCAAAGAC
92	ACCACGGAATAAGTTTATTTTGTCACAATCAATAGAAA
93	ATTCATATGGTTTACCAGCGCCAAAGACAAAAGGGCGA
94	CATTCAACCGATTGAGGGAGGGAAGGTAAATATTGACG
95	GAAATTATTCATTAAAGGTGAATTATCACCGTCACCGA
96	CTTGAGCCATTTGGGAATTAGAGCCAGCAAAATCACCA
97	GTAGCACCATTACCATTAGCAAGGCCGGAAACGTCACC
98	AATGAAACCATCGATAGCAGCACCGTAATCAGTAGCGA
99	CAGAATCAAGTTTGCCTTTAGCGTCAGACTGTAGCGCG
100	TTTTCATCGGCATTTTCGGTCATAGCCCCCTTATTAGC
101	GTTTGCCATCTTTTCATAATCAAAATCACCGGAACCAG
102	AGCCACCACCGGAACCGCCTCCCTCAGAGCCGCCACCC
103	TCAGAACCGCCACCCTCAGAGCCACCACCCTCAGAGCC
104	GCCACCAGAACCACCACCAGAGCCGCCGCCAGCATTGA
105	CAGGAGGTTGAGGCAGGTCAGACGATTGGCCTTGATAT
106	TCACAAACAAATAAATCCTCATTAAAGCCAGAATGGAA
107	AGCGCAGTCTCTGAATTTACCGTTCCAGTAAGCGTCAT
108	ACATGGCTTTTGATGATACAGGAGTGTACTGGTAATAA
109	GTTTTAACGGGGTCAGTGCCTTGAGTAACAGTGCCCGT
110	ATAAACAGTTAATGCCCCCTGCCTATTTCGGAACCTAT
111	TATTCTGAAACATGAAAGTATTAAGAGGCTGAGACTCC
112	TCAAGAGAAGGATTAGGATTAGCGGGGTTTTGCTCAGT
113	ACCAGGCGGATAAGTGCCGTCGAGAGGGTTGATATAAG
114	TATAGCCCGGAATAGGTGTATCACCGTACTCAGGAGGT
115	TTAGTACCGCCACCCTCAGAACCGCCACCCTCAGAACC
116	GCCACCCTCAGAGCCACCACCCTCATTTTCAGGGATAG
117	CAAGCCCAATAGGAACCCATGTACCGTAACACTGAGTT
118	TCGTCACCAGTACAAACTACAACGCCTGTAGCATTCCA
119	CAGACAGCCCTCATAGTTAGCGTAACGATCTAAAGTTT
120	TGTCGTCTTTCCAGACGTTAGTAAATGAATTTTCTGTA
121	TGGGATTTTGCTAAACAACTTTCAACAGTTTCAGCGGA
122	GTGAGAATAGAAAGGAACAACTAAAGGAATTGCGAATA
123	ATAATTTTTTCACGTTGAAAATCTCCAAAAAAAAGGCT
124	CCAAAAGGAGCCTTTAATTGTATCGGTTTATCAGCTTG
125	CTTTCGAGGTGAATTTCTTAAACAGCTTGATACCGATA
126	GTTGCGCCGACAATGACAACAACCATCGCCCACGCATA
127	ACCGATATATTCGGTCGCTGAGGCTTGCAGGGAGTTAA
128	AGGCCGCTTTTGCGGGATCGTCACCCTCAGCAGCGAAA
129	GACAGCATCGGAACGAGGGTAGCAACGGCTACAGAGGC
130	TTTGAGGACTAAAGACTTTTTCATGAGGAAGTTTCCAT
131	TAAACGGGTAAAATACGTAATGCCACTACGAAGGCACC
132	AACCTAAAACGAAAGAGGCAAAAGAATACACTAAAACA
133	CTCATCTTTGACCCCCAGCGATTATACCAAGCGCGAAA
134	CAAAGTACAACGGAGATTTGTATCATCGCCTGATAAAT
135	TGTGTCGAAATCCGCGACCTGCTCCATGTTACTTAGCC
136	GGAACGAGGCGCAGACGGTCAATCATAAGGGAACCGAA
137	CTGACCAACTTTGAAAGAGGACAGATGAACGGTGTACA

138	GACCAGGCGCATAGGCTGGCTGACCTTCATCAAGAGTA
139	ATCTTGACAAGAACCGGATATTCATTACCCAAATCAAC
140	GTAACAAAGCTGCTCATTCAGTGAATAAGGCTTGCCCT
141	GACGAGAAACACCAGAACGAGTAGTAAATTGGGCTTGA
142	GATGGTTTAATTTCAACTTTAATCATTGTGAATTACCT
143	TATGCGATTTTAAGAACTGGCTCATTATACCAGTCAGG
144	ACGTTGGGAAGAAAAATCTACGTTAATAAAACGAACTA
145	ACGGAACAACATTATTACAGGTAGAAAGATTCATCAGT
146	TGAGATTTAGGAATACCACATTCAACTAATGCAGATAC
147	ATAACGCCAAAAGGAATTACGAGGCATAGTAAGAGCAA
148	CACTATCATAACCCTCGTTTACCAGACGACGATAAAAA
149	CCAAAATAGCGAGAGGCTTTTGCAAAAGAAGTTTTGCC
150	AGAGGGGGTAATAGTAAAATGTTTAGACTGGATAGCGT
151	CCAATACTGCGGAATCGTCATAAATATTCATTGAATCC
152	CCCTCAAATGCTTTAAACAGTTCAGAAAACGAGAATGA
153	CCATAAATCAAAAATCAGGTCTTTACCCTGACTATTAT
154	AGTCAGAAGCAAAGCGGATTGCATCAAAAAGATTAAGA
155	GGAAGCCCGAAAGACTTCAAATATCGCGTTTTAATTCG
156	AGCTTCAAAGCGAACCAGACCGGAAGCAAACTCCAACA
157	GGTCAGGATTAGAGAGTACCTTTAATTGCTCCTTTTGA
158	TAAGAGGTCATTTTTGCGGATGGCTTAGAGCTTAATTG
159	CTGAATATAATGCTGTAGCTCAACATGTTTTAAATATG
160	CAACTAAAGTACGGTGTCTGGAAGTTTCATTCCATATA
161	ACAGTTGATTCCCAATTCTGCGAACGAGTAGATTTAGT
162	TTGACCATTAGATACATTTCGCAAATGGTCAATAACCT
163	GTTTAGCTATATTTTCATTTGGGGCGCGAGCTGAAAAG
164	GTGGCATCAATTCTACTAATAGTAGTAGCATTAACATC
165	CAATAAATCATACAGGCAAGGCAAAGAATTAGCAAAAT
166	TAAGCAATAAAGCCTCAGAGCATAAAGCTAAATCGGTT
167	GTACCAAAAACATTATGACCCTGTAATACTTTTGCGGG
168	AGAAGCCTTTATTTCAACGCAAGGATAAAAATTTTTAG
169	AACCCTCATATATTTTAAATGCAATGCCTGAGTAATGT
170	GTAGGTAAAGATTCAAAAGGGTGAGAAAGGCCGGAGAC
171	AGTCAAATCACCATCAATATGATATTCAACCGTTCTAG
172	CTGATAAATTAATGCCGGAGAGGGTAGCTATTTTTGAG
173	AGATCTACAAAGGCTATCAGGTCATTGCCTGAGAGTCT
174	GGAGCAAACAAGAGAATCGATGAACGGTAATCGTAAAA
175	CTAGCATGTCAATCATATGTACCCCGGTTGATAATCAG
176	AAAAGCCCCAAAAACAGGAAGATTGTATAAGCAAATAT
177	TTAAATTGTAAACGTTAATATTTTGTTAAAATTCGCAT
178	TAAATTTTTGTTAAATCAGCTCATTTTTTAACCAATAG
179	GAACGCCATCAAAAATAATTCGCGTCTGGCCTTCCTGT
180	AGCCAGCTTTCATCAACATTAAATGTGAGCGAGTAACA
181	ACCCGTCGGATTCTCCGTGGGAACAAACGGCGGATTGA
182	CCGTAATGGGATAGGTCACGTTGGTGTAGATGGGCGCA
183	TCGTAACCGTGCATCTGCCAGTTTGAGGGGACGACGAC
184	AGTATCGGCCTCAGGAAGATCGCACTCCAGCCAGCTTT

185	CCGGCACCGCTTCTGGTGCCGGAAACCAGGCAAAGCGC
186	CATTCGCCATTCAGGCTGCGCAACTGTTGGGAAGGGCG
187	ATCGGTGCGGGCCTCTTCGCTATTACGCCAGCTGGCGA
188	AAGGGGGATGTGCTGCAAGGCGATTAAGTTGGGTAACG
189	CCAGGGTTTTCCCAGTCACGACGTTGTAAAACGACGGC
190	CAGTGCCAAGCTTGCATGCCTGCAGGTCGACTCTAGAGGATCTTTT

Supplementary Table S3. Oligonucleotides were replaced from Table S2 to assemble reference structures. The DNA dumbbell forming sequence is indicated in red.

Name	Sequence (5' → 3')	Length (nt)	# of oligos replaced
REF 1.1	ACATCACTTGCCTGAGTAGA	20	26-30

REF 1.2	AGAACTCAAATCCTCTTTTGAGGAACAAGTTTTCTTGTCTATCGGCCT	48	
REF 1.3	TGCTGGTAATTCCTCTTTTGAGGAACAAGTTTTCTTGTATCCAGAACA	48	
REF 1.4	ATATTACCGCTCCTCTTTTGAGGAACAAGTTTTCTTGTCAGCCATTGC	48	
REF 1.5	AACAGGAAAATCCTCTTTTGAGGAACAAGTTTTCTTGTACGCTCATGG	48	
REF 1.6	AAATACCTACTCCTCTTTTGAGGAACAAGTTTTCTTGTATTTTGACGC	48	
REF 1.7	TCAATCGTCTTCCTCTTTTGAGGAACAAGTTTTCTTGTGAAATGGATT	48	
REF 1.8	ATTTACATTGGCAGATTCAC	20	
REF 1.9	CAGTCACACGACCAGTAATAAAAGGGACAT	30	
REF 2.1	TCACAAACAAATAAATCCTCATTAAAGCCAGAATGGAAAGCGCAGTCTCTGAATTT	56	106-112
REF 2.2	ACCGTTCCAGTAAGCGTCAT	20	
REF 2.3	ACATGGCTTTTCCTCTTTTGAGGAACAAGTTTTCTTGTTGATGATACA	48	
REF 2.4	GGAGTGTACTTCCTCTTTTGAGGAACAAGTTTTCTTGTGGTAATAAGT	48	
REF 2.5	TTTAACGGGGTCCTCTTTTGAGGAACAAGTTTTCTTGTTCAGTGCCTT	48	
REF 2.6	GAGTAACAGTTCCTCTTTTGAGGAACAAGTTTTCTTGTGCCCGTATAA	48	
REF 2.7	ACAGTTAATGTCCTCTTTTGAGGAACAAGTTTTCTTGTCCCCCTGCCT	48	
REF 2.8	ATTTCGGAACTCCTCTTTTGAGGAACAAGTTTTCTTGTCTATTATTCT	48	
REF 2.9	GAAACATGAAAGTATTAAGA	20	
REF 2.10	GGCTGAGACTCCTCAAGAGAAGGATTAGGATTAGCGGGGTTTTGCTCAGT	50	

Section S4. AFM imaging

Section 4.1 Sample preparation and imaging with AFM

Atomic Force Microscopy (Nanosurf Mobile S) imaging of nanobaits was performed in the air in a non-contact mode. All scans were performed on a bare mica surface following the adsorption of nanobaits as follows. We placed a 10 μL drop of a DNA solution (diluted to 1 ng/μL in filtered 10 mM $MgCl_2$ and 10 mM Tris-HCl, pH 8.0) onto a freshly cleaved mica surface for 1 minute, rinsed the mica plate three times with 100 μL of Mili-Q water and then blow-dried it with Nitrogen. Before the scan, the mica plate was affixed to the AFM sample stage using double-sided adhesive tape. Image visualization and analysis were done using Gwyddion.

Section 4.2 AFM images of nanobait

AFM images of nanobait are shown in Figures S3 and S4. Figure S3a presents AFM images of the nanobait structure without any label added. In some cases, two references are visible (circled in dark grey, Figure S3a, right). However, it is known that DNA dumbbell structures are hardly distinguishable with AFM imaging in comparison to nanopores [1].

Nanobait events with monovalent streptavidin (Figure S3b) indicate five structures that correspond to capture sites with labels, as expected from the nanobait design. The same design but with the DNA flower label is presented in Figure S4. The DNA flower is larger than streptavidin and hence easier to be detected using AFM imaging (Figure S2).

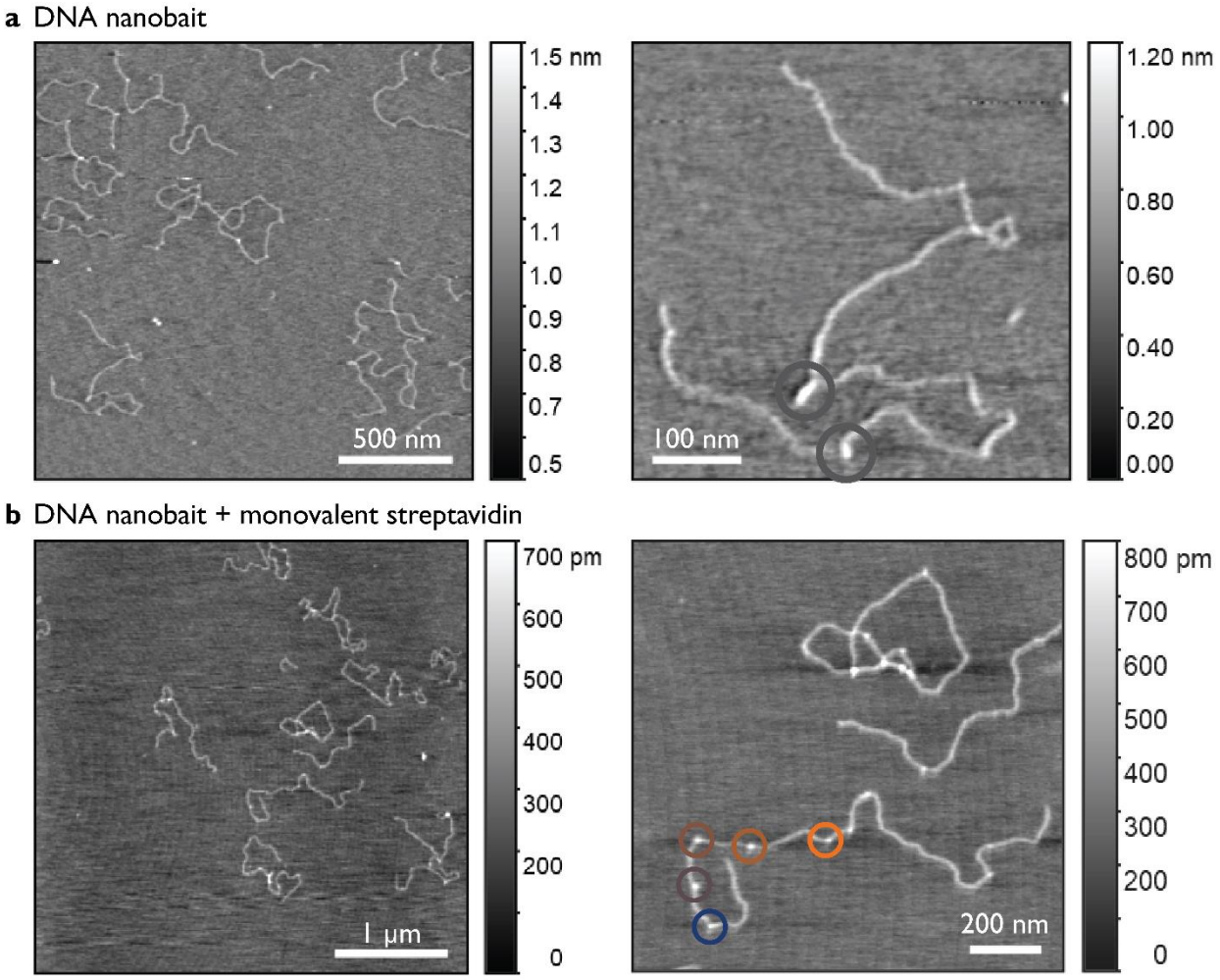

Figure S3. AFM images of DNA nanobait (as in Figure 3) with monovalent streptavidin. a) Nanobait without monovalent streptavidin has two reference structures (circled in dark gray). b) AFM images of nanobait with monovalent streptavidin used as a label. Five capture sites are circled in corresponding colors. Five non-overlapping areas are imaged for each sample.

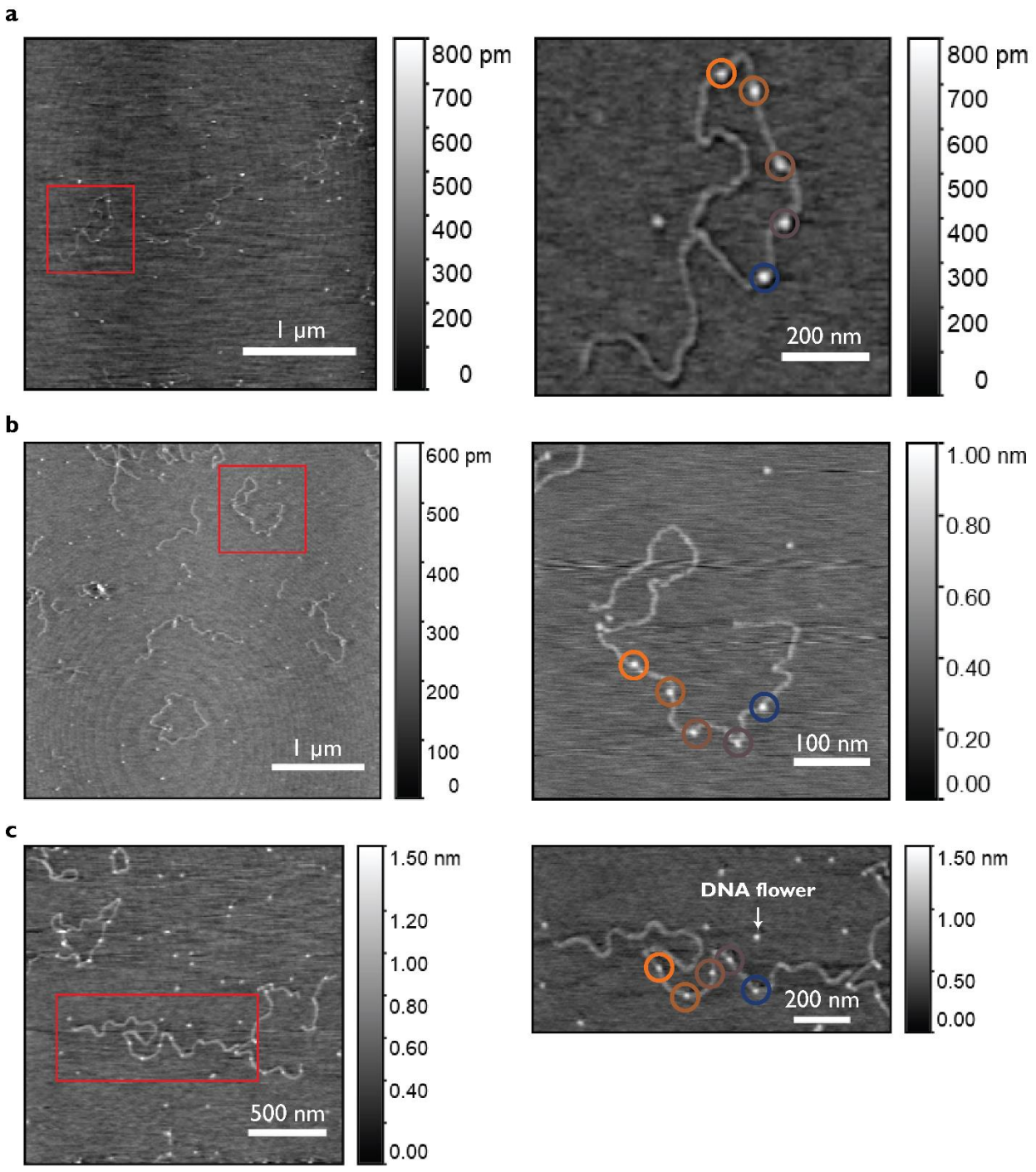

Figure S4. AFM images of nanobait (as in Figure 3) with DNA flower as a label. Three different nanobait example images are shown in a), b), and c). Five non-overlapping areas are imaged for each sample.

Section S5. EMSA analysis

We performed the electrophoretic mobility shift assay (EMSA) to see a mobility shift caused by streptavidin binding to all five sites on nanobait (Figure S5). 2 % (w/v) agarose (BioReagent, low electroendosmosis, Merck SigmaAldrich; catalog number A9539) gel was prepared by adding 2 g of agarose, 10 mL of 10 × Tris-Borate-EDTA buffer (TBE buffer), and Milli-Q water was added to 100 mL. The gel was heated in the microwave at the maximum power (800 W) for 2-3 min. It was cooled down and poured into a gel tray to set for 45 min.

Samples were mixed with purple gel loading dye (New England Biolabs; catalog number B7025S) and TBE buffer to 1 × with ~150 ng of a DNA sample. We used a 1 kb DNA ladder as a reference (New England Biolabs; catalog number N3232) with a size range from 500 bp to 10 kb (Figure S5a). Nanobait in lane 2 (Figure S5a) was mixed with 10 × excess of wild-type tetravalent streptavidin (ThermoFisher Scientific; catalog number 21125).

It can be observed from the agarose gel in Figure S5a that there is a slight shift from nanobait (lane 1) to nanobait + streptavidin (lane 2). We used gel intensity analysis using an open-source software Fiji[8] to plot this shift, indicating that streptavidin(s) is bound to nanobait (Figure S5b).

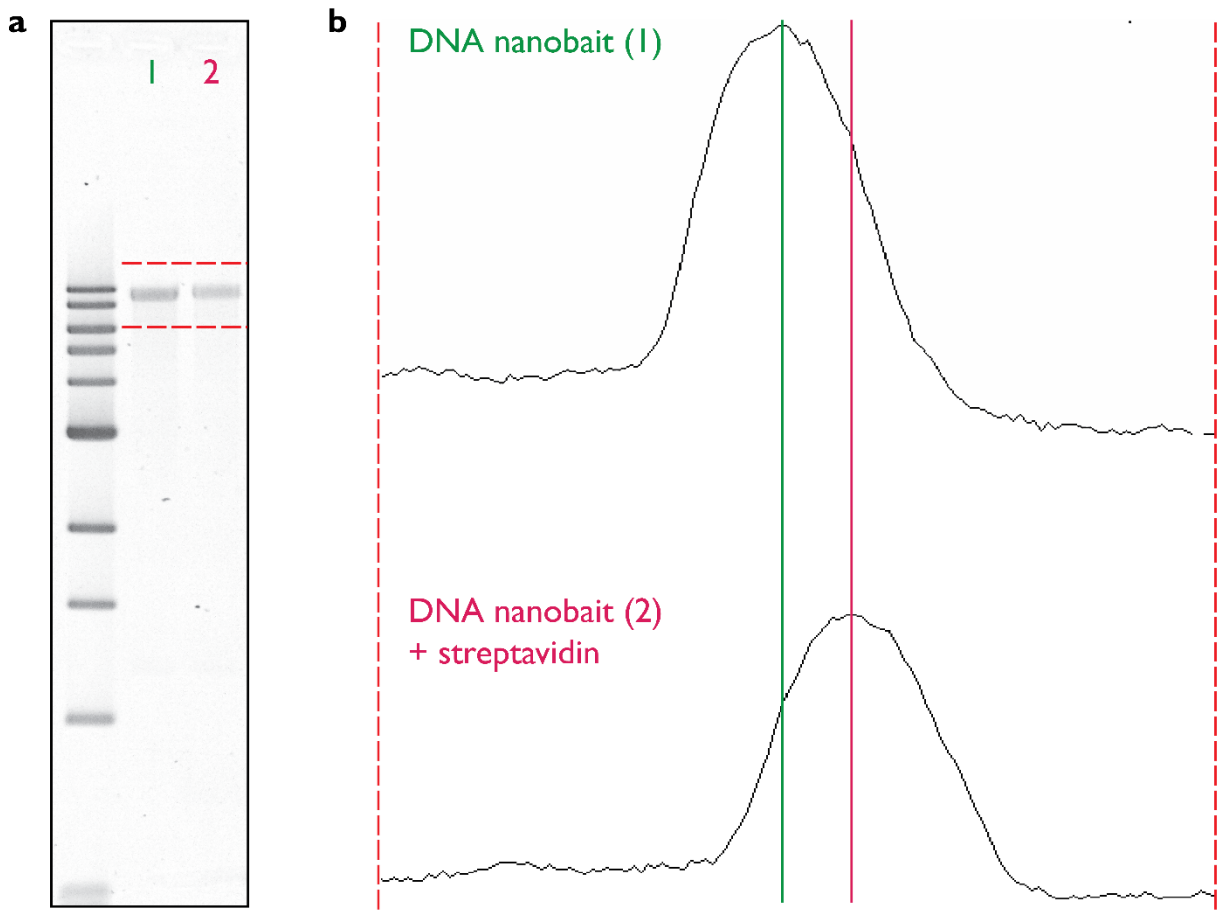

Figure S5. Electrophoretic mobility shift assay (EMSA) of nanobait without and with streptavidin. a) 2% (w/v) agarose gel od nanobait without (lane 1) and with (lane 2) streptavidin added. We used a 1 kb DNA ladder (New England Biolabs; product number N3232). The two top lines of the ladder are 10 and 8 kb. b) The intensity traces of corresponding lanes from a). The green line indicates the intensity maximum of nanobait (lane 1) and the purple line indicates the intensity maximum of nanobait + streptavidin (lane 2). The shift between the green and purple lines corresponds to streptavidin(s) bound to capture sites on nanobait. Samples were run once.

Section S6. Multiple respiratory viruses DNA nanobait sequences and example events

Nanobait for multiple respiratory viruses is prepared as previously described in Section S2. Below, are listed sequences of capture sites (Table S7), biotin strand (Table S6), and target sequence (Table S5) for each virus.

We also show here additional nanopore events of nanobait without target added (Figure S6a), with SARS-CoV-2 target (Figure S6b), Influenza A (Figure S6c), RSV (Figure S6d), Parainfluenza (Figure S6e), and Rhinoviruses (Figure S6f). Targets for Influenza A, Parainfluenza A, and Rhinoviruses target cohort rather than a single variant [9,10]. The nanobait and peaks resemble those presented in Figure 2a of the manuscript. These single-molecule events are obtained from three separate nanopore measurements.

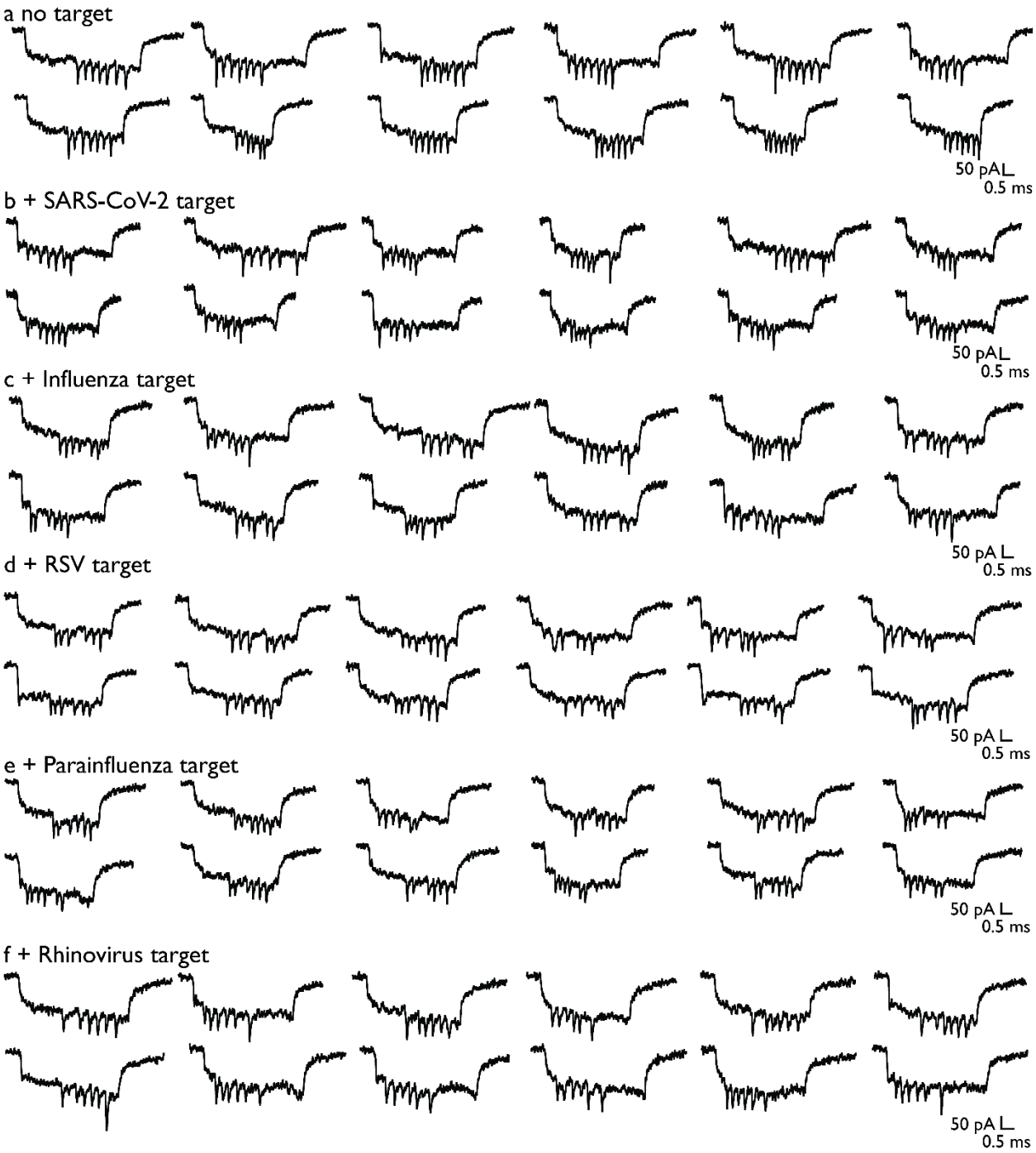

Figure S6. Additional example events for nanobait used for identification of various respiratory viruses with a) no target added, b) SARS-CoV-2 target, c) Influenza target, d) RSV, e) Parainfluenza target, and f) Rhinovirus target.

Supplementary Table S4. Presence of peaks at their respective sites for multiple virus identification.

Target/Case	Control (no targets)	Standard error	Target present	Standard error
SARS-CoV-2	0.17	0.04	0.75	0.10
RSV	0.09	0.01	0.96	0.06
Rhinovirus	0.08	0.03	0.89	0.13
Influenza	0.11	0.04	0.49	0.17
Parainfluenza	0.03	0.01	0.73	0.04

Supplementary Table S5. Target sequences for multiple virus identification.

Strand name	Virus / group of viruses	Sequence reference	Sequence (5' → 3')
SW	SARS-CoV-2_Reference	NCBI Reference Sequence: NC_045512.2[11]	GTATGAAAATGCCTTTTTAC
Infl	Influenza A viruses universal	Sequence adapted from[12]	TGACAGGATTGGTCTTGTCT
RSV	Respiratory syncytial virus universal A	Sequence adapted from[13]	ACACAGCAGCTGTTCAGTAC
PI	Parainfluenza 1	Sequence adapted from[10]	CTTCCTGCTGGTGTGTTAAT
RV	Rhinoviruses universal	Sequence adapted from[9]	TCCTCCGGCCCCTGAATGTG

Supplementary Table S6. 3' biotinylated strand sequences for multiple virus identification.

Strand name	Virus / group of viruses	Sequence (5' → 3')
bSW	SARS-CoV-2_Reference	AAATGCCTTTTTAC/3-biotin/
bInfl	Influenza A viruses universal	GATTGGTCTTGTCT/3-biotin/
bRSV	Respiratory syncytial virus universal A	CAGCTGTTCAGTAC/3-biotin/
bPI	Parainfluenza 1	GCTGGTGTGTTAAT/3-biotin/

bRV	Rhinoviruses universal	GGCCCCTGAATGTG /3-biotin/

Supplementary Table S7. Capture strand sequences for multiple virus identification.

Strand name	Virus / group of viruses	Sequence (5' → 3')
cSW_42	SARS-CoV-2_Reference	TTCGACAACTCGTATTAAATCCTTTGCCCGAACGTTAT TTTTT GTAAAAAGGCATTTTCATAC
cRSV_55	Respiratory syncytial virus universal A	GTGAGTGAATAACCTTGCTTCTGTAAATCGTCGCTATT TTTTT GTACTGAACAGCTGCTGTGT
cRV_68	Rhinoviruses universal	AGAATATAAAGTACCGACAAAAGGTAAAGTAATTCTGT TTTTT CACATTCAGGGGCCGGAGGA
cI_81	Influenza A viruses universal	TCCCAATCCAAATAAGAAACGATTTTTTGTTTAACGTC TTTTT AGACAAGACCAATCCTGTCA
cPI_94	Parainfluenza 1	CATTCAACCGATTGAGGGAGGGAAGGTAAATATTGACG TTTTT ATTAACACACCAGCAGGAAG

Section S7. Multiple SARS-Co-V-2 virus variants DNA nanobait sequences and example events

Nanobait for multiple SARS-CoV-2 variants was prepared as previously described in Section S2. Below are listed sequences of capture sites (Table S12), biotin strand (Table S10), and target sequence of the wildtype (Table S11) and variant (Table S9).

We also showed here additional nanopore events of nanobait without target added (Figure S7a), with B reference target (Figure S7b), B.1.617 variant target (Figure S7c), B.1 variant target (Figure S7d), B.1.1.7 variant target (Figure S7e), and B.1.351 variant target (Figure S7f). The nanobait and peaks resembled those presented in Figure 2b of the manuscript. These single-molecule events were obtained from three separate nanopore measurements.

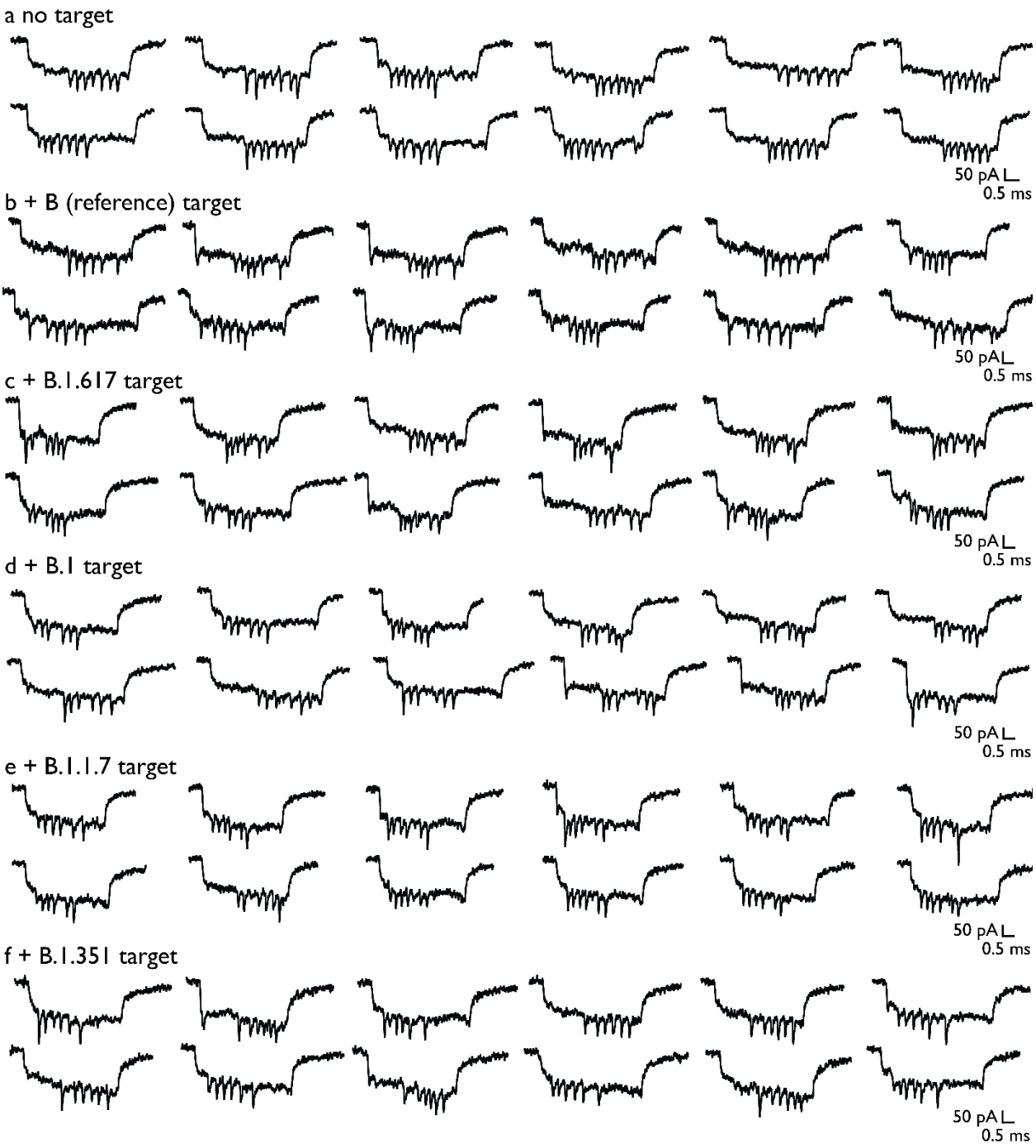

Figure S7. Additional example events for nanobait used for identification of various SARS-CoV-2 variants with a) no target added, b) B target, c) B.1.617 variant target, d) B.1 variant target, e) B.1.1.7 variant target, and f) B.1.351 variant target.

Supplementary Table S8. Presence of peaks at their respective sites for multiple variant identification.

Target/Case	Control (no targets)	Standard error	WT target present	Standard error	Variant target present	Standard error
B (reference)	0.08	0.00	0.93	0.04	0.92	0.06
B.1.617 (Delta)	0.23	0.01	0.39	0.02	0.77	0.01
B.1	0.02	0.00	0.29	0.05	0.98	0.06
B.1.1.7 (Alpha)	0.04	0.00	0.06	0.02	0.96	0.12
B.1.351 (Beta)	0.10	0.00	0.49	0.11	0.90	0.03

Supplementary Table S9. Target sequences for multiple SARS-CoV-2 variant identification. In red, single nucleotide variant positions are highlighted, while yellow highlights the toehold region used for the SDR.

Strand name	WHO nomenclature[14]	Pangolin nomenclature[15]	Single nucleotide variation	Sequence (5' → 3')
SW	Reference	B (reference)	/	GTATGAAAATGCCTTTTTAC
SIm	Delta	B.1.617	T-G L452R	CCGGTATAGATTGTTTAGGA
SEm	NA	B.1	A-G D614G	GGTGTTAACTGCACAGAAGT
SUKm	Alpha	B.1.1.7	A-T N501Y	CTTATGGTGTTGGTTACCAA
SSAm	Beta	B.1.351	G-A E484K	TAAAGGTTTTAATTGTTACT

Supplementary Table S10. 3' biotinylated strand sequences for multiple SARS-CoV-2 variant identification.

Strand name	Variant name	Sequence (5’ → 3’)
bSW	B (reference)	AAATGCCTTTTTAC/3-BIOTIN/
bSIm	B.1.617 (Delta)	TAGATTGTTTAGGA/3-BIOTIN/
bSEm	B.1	AACTGCACAGAAGT/3-BIOTIN/
bSUKm	B.1.1.7 (Alpha)	GTGTTGGTTACCAA/3-BIOTIN/
bSSAm	B.1.351 (Beta)	TTTTAATTGTTACT/3-BIOTIN/

Supplementary Table S11. Wild-type (WT) target sequences for multiple SARS-CoV-2 variant identification. In green, wild-type nucleotide positions are highlighted, while yellow highlights the toehold region used for the SDR.

Strand name	Sequence (5’ → 3’)	Length (nt)
SI	CCTGTATAGATTGTTTAGGA	20
SE	GATGTTAACTGCACAGAAGT	20
SUK	CTAATGGTGTTGGTTACCAA	20
SSA	TGAAGGTTTTAATTGTTACT	20

Supplementary Table S12. Capture strand sequences for multiple SARS-CoV-2 variant identification.

Strand name	Variant name	Sequence (5’ → 3’)
cSW_42	B (reference)	TTCGACAACTCGTATTAAATCCTTTGCCCGAACGTTAT TTTTT GTAAAAAGGCATTTTCATAC
cSI_68	B.1.617 (Delta)	AGAATATAAAGTACCGACAAAAGGTAAAGTAATTCTGT TTTTT TCCTAAACAATCTATACCGG
cSE_94	B.1	CATTCAACCGATTGAGGGAGGGAAGGTAAATATTGACG TTTTT ACTTCTGTGCAGTTAACACC
cSUK_81	B.1.1.7 (Alpha)	TCCCAATCCAAATAAGAAACGATTTTTTGTTTAACGTC TTTTT TTGGTAACCAACACCATAAG

cSSA_55	B.1.351 (Beta)	GTGAGTGAATAACCTTGCTTCTGTAAATCGTCGCTATT TTTTT AGTAACAATTAAAACCTTTA

Section S8. Discrimination of control SARS-Co-V-2 RNA virus variants

Nanobait for SARS-CoV-2 N501 RNA virus variants was prepared as previously described in Section S2 (Figure S8). Below, are listed sequences of SARS-CoV-2 N501 RNA, capture sites, biotinylated strand, and guide oligos used for RNase H cutting (Table S13).

Programmable RNase H cutting of SARS-CoV-2 RNA controls for nanobait

For nanopore sensing, SARS-CoV-2 RNA (S:N501 in Table S13) controls were used for the detection with nanobait. Firstly, we mixed guide oligos with a SARS-CoV-2 N501 RNA in the ratio 1:1:1 and heated the mixture to 70 °C for 5 minutes. RNase H (5,000 units/ml, NEB) was added, mixed, and heated for 20 minutes at 37 °C to allow the enzyme to cut RNA in the DNA : RNA hybrid that effectively leads to the release of target RNA. RNase H is thermally inactivated by incubation at 65 °C for 10 min.

Nanopore readout of DNA nanobait

Nanobait was mixed with a cut long RNA control at ten times excess in 10 mM $MgCl_2$ and 100 mM NaCl. The mixture (5 µL) was incubated at room temperature (~10 min) until prepared for nanopore measurement.

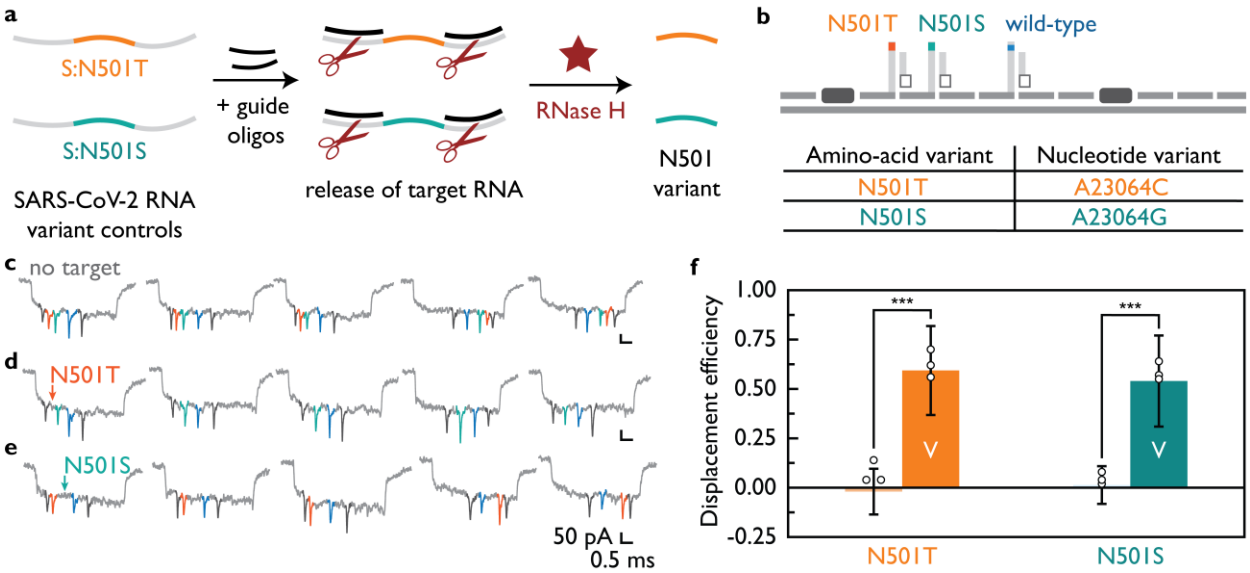

Figure S8. Nanobait discriminates single-nucleotide SARS-CoV-2 RNA variants. a) SARS-CoV-2 RNA variant controls that have one amino-acid substitutions. Guide oligos are added next to the target RNA sequence hence enabling RNase H cutting and releasing of target RNAs in solution. b) Nanobait design has two references, two sites for each of variant (N501T, N501S) and a wild-type site. In the table each of these amino-acid variants are shown with position and substitution of nucleotide counterpart indicated. c)

Example events for no target control indicate the correct number of downward spikes each corresponding to a structure depicted in b). In d) and e) are shown example events for each of the N501 variants. The absence of the colored spike indicates the presence of each respective target. f) Displacement efficiencies for single-nucleotide SARS-CoV-2 variants (labelled as 'V') are compared with the displacement efficiency for the wild-type SARS-CoV-2 (B.1.1.7). Error bars represent standard error and the center as the mean for three nanopore measurements and fifty nanopore events per measurement. The difference between conditions without and with variant targets is statistically significant (***p < 0.001; two-sided Student's T test; N=150).

Supplementary Table S13. SARS-CoV-2 RNA sequences and guide oligos, capture sites and biotinylated strands.

Strand name	Description	Sequence (5' → 3')
S:N501_RNA	Wild-type oligo	ATCATATGGTTTCCAACCCA CTTATGGTGTTGGTTACCAA CCATACAGAGTAGTAGTACT
S:N501T_RNA	A23064C	ATCATATGGTTTCCAACCCA CTTCTGGTGTTGGTTACCAA CCATACAGAGTAGTAGTACT
S:N501S_RNA	A23064G	ATCATATGGTTTCCAACCCA CTTGTGGTGTTGGTTACCAA CCATACAGAGTAGTAGTACT
Guide oligo S:N501_a	Downstream cutting oligo	TGGGTTGGAAACCATATGAT
Guide oligo S:N501_b	Upstream cutting oligo	AGTACTACTACTCTGTATGG
cS42:N501T	Carrier overhang	TTCGACAACTCGTATTAAATCCTTTGCCCGAACGTTAT TTTTT
cS55:N501S	Carrier overhang	GTGAGTGAATAACCTTGCTTCTGTAAATCGTCGCTATT TTTTT
cSUK_81	Carrier overhang	TCCCAATCCAAATAAGAAACGATTTTTTGTTTAACGTC TTTTT TTGGTAACCAACACCAAAAG
bS:N501	Biotin	GTGTTGGTTACCAA/3-BIOTIN/

Section S9. Kinetics of SDR with DNA and RNA targets

Nanobait for multiple SARS-CoV-2 targets is prepared as previously described in Section S2. Below, are listed sequences of capture sites (Table S17), biotin strands (Table S16), and target strands (Table S15).

Kinetics measurements for all five targets SDR are shown in Figure S9 and fifty nanobait events are analyzed per each data point. We tested targets of the same sequence but with different backbones as RNAs or DNAs (Figure S9a and S9b, respectively). Here, we show that target chemistry might have an effect on the kinetics of the SDR since some of the targets (e.g. target 3) have slower SDR for the RNA sequence than compared to the DNA sequence.

Additional nanopore events of nanobait without any target added (Figure S9c) and all five targets present (Figure S9d).

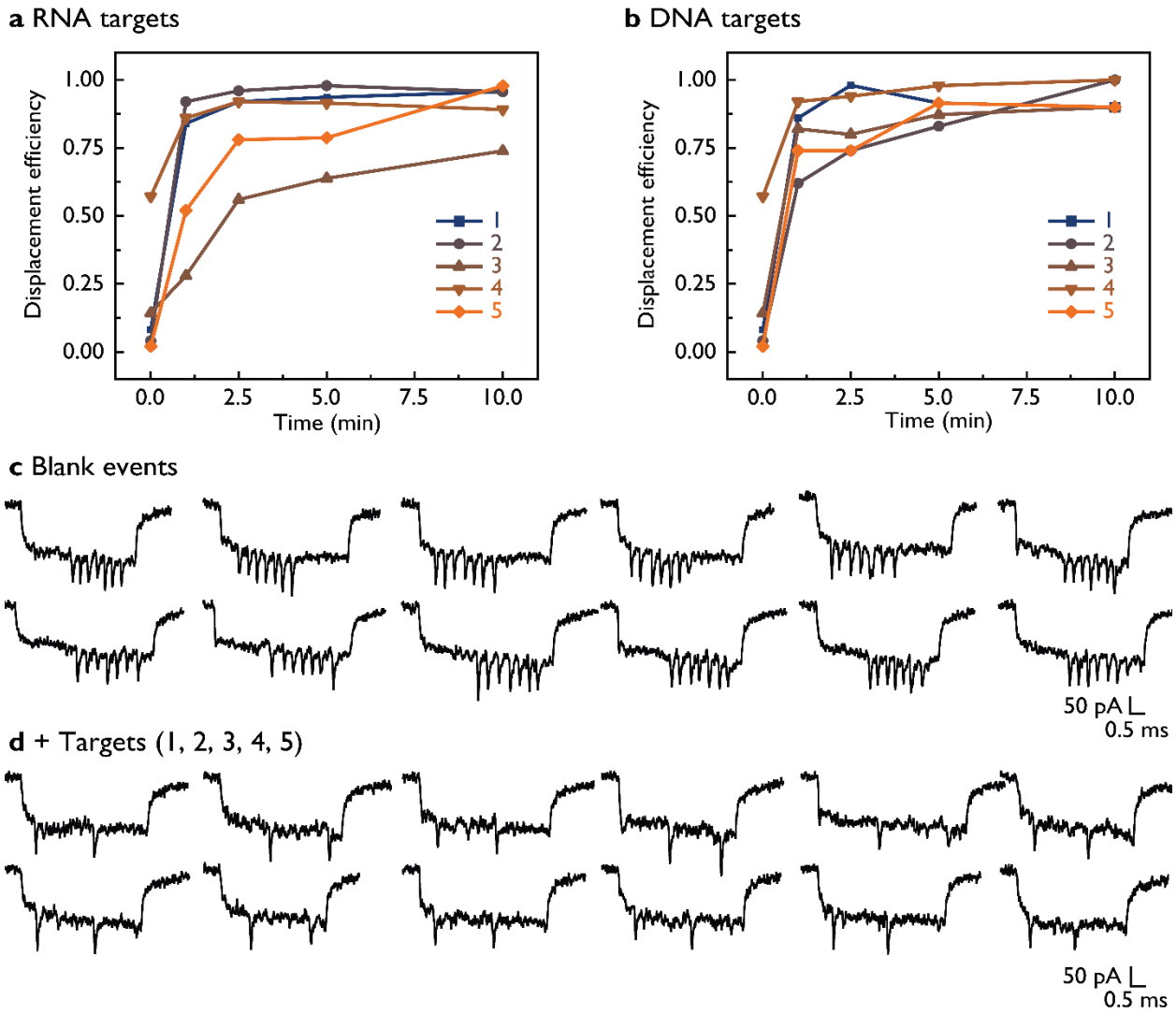

Figure S9. Kinetics of the toehold strand-displacement reaction (SDR) using RNA and DNA targets. Displacement efficiency for five different RNA or DNA targets is plotted in a) and b), respectively. c) Blank (no targets added) nanopore events indicate correct nanobait assembly. d) After the SDR with five targets added all five target-specific downward signals diminish.

We have measured single-molecule kinetics of SDR over 9 h for RNA targets (Figure S10). This experiment is performed with the diluted nanobait sample and in 1:1 ratio nanobait to target and allowed the typical 10 min incubation for the SDR. We have obtained from 1150 to 2860 events per hour slot (~18000 events) and the first fifty events were analyzed after each hour and the average value is plotted in Figure S10.

We can observe a general trend of increasing displacement efficiency for all five targets (Figure S10).

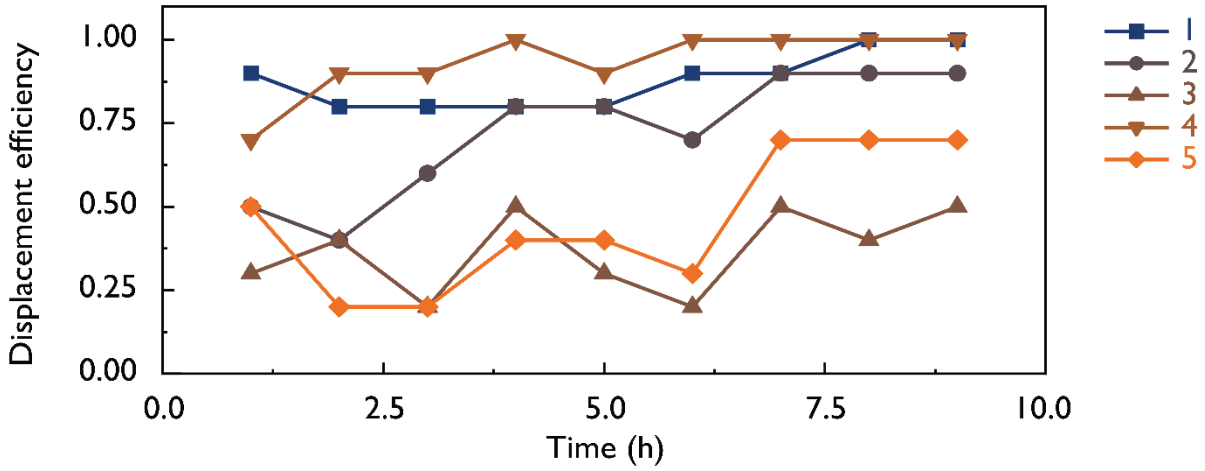

Figure S10. Single-molecule kinetics of the toehold strand-displacement reaction (SDR) using RNA targets.

Supplementary Table S14. Presence of peaks at their respective sites for multiple SARS-CoV-2 target identification.

Target/Case	Control (no targets)	Standard error	Target present	Standard error
H1	0.08	0.14	0.92	0.08
H2	0.10	0.16	0.90	0.22
H3	0.13	0.18	0.87	0.14
H4	0.38	0.11	0.62	0.08
H5	0.08	0.14	0.92	0.12

Supplementary Table S15. Target sequences for multiple SARS-CoV-2 target identification.

Strand name	Sequence (5' → 3')	Length (nt)

H1	TGATTGTGAAGAAGAAGAGT	20
H2	AAGAAAGGAGCTAAATTGTT	20
H3	AGAGTTGATTTTTGTGGAAA	20
H4	TGGTGTTTATTCTGTTATTT	20
H5	GGTAAAGTTGAGGGTTGTAT	20

Supplementary Table S16. 3’ Biotinylated strand sequences for SARS-CoV-2 target identification in a patient sample.

Strand name	Sequence (5’ → 3’)	Length (nt)
bH1	TGAAGAAGAAGAGT /3’-biotin/	14
bH2	GGAGCTAAATTGTT /3’-biotin/	14
bH3	GATTTTTGTGGAAA /3’-biotin/	14
bH4	TTATTCTGTTATTT /3’-biotin/	14
bH5	GTTGAGGGTTGTAT /3’-biotin/	14

Supplementary Table S17. Capture strand sequences for the multiple SARS-CoV-2 target identification.

Strand name	Sequence (5’ → 3’)	Length (nt)
cH1_42	TTCGACAACTCGTATTAAATCCTTTGCCCGAACGTTAT TTTTT ACTCTTCTTCTTCACAATCA	63
cH2_55	GTGAGTGAATAACCTTGCTTCTGTAAATCGTCGCTATT TTTTT AACAATTTAGCTCCTTTCTT	63
cH3_68	AGAATATAAAGTACCGACAAAAGGTAAAGTAATTCTGT TTTTT TTTCCACAAAAATCAACTCT	63

cH4_81	TCCCAATCCAAATAAGAAACGATTTTTTGTTTAACGTC TTTTT AAATAACAGAATAAACACCA	63
cH5_94	CATTCAACCGATTGAGGGAGGGAAGGTAAATATTGACG TTTTT ATACAACCCTCAACTTTACC	63

Section S10. Gel analysis of MS2 RNA cutting

Oligonucleotides A and B (Figure 4c) correspond to guide oligos TXA and TXB (X being the target name). Oligo C corresponds to cTX (X being the target name).

We treated MS2 RNA with a single target or with all three targets together to visualize site-specific cutting of RNA. We analyzed these samples using agarose gel electrophoresis (Figure S11). After MS2 RNA cutting for all three sites, we can observe expected lane mobility.

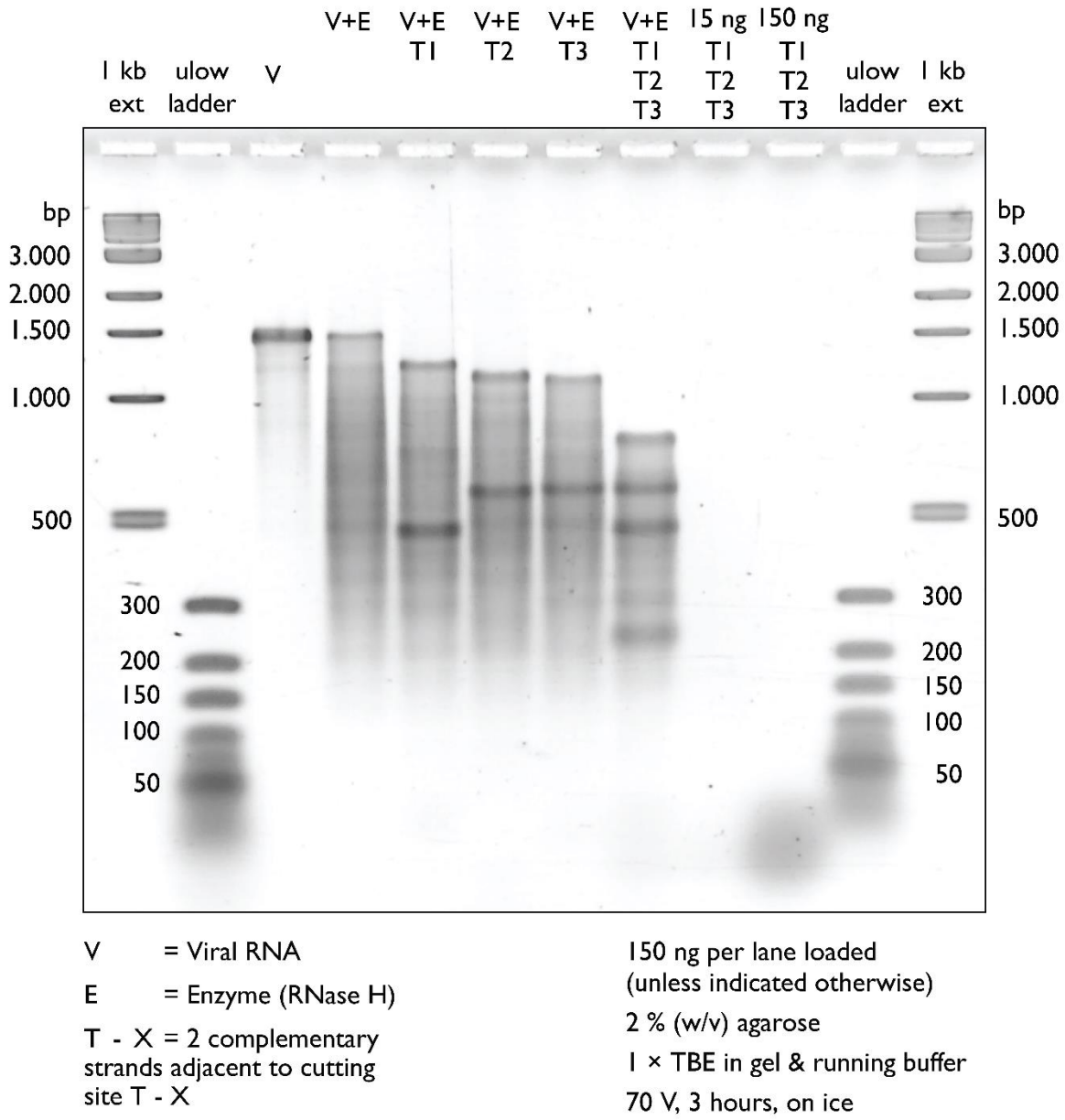

Figure S11. Agarose gel analysis of RNase H cutting of MS2 viral RNA.

We tested the mobility of targets, guide oligos, and capture oligos with non-denaturing polyacrylamide gel electrophoresis (PAGE) analysis (Figure S12). Despite targets and guide oligos having the same length they have different band mobility. This result indicates that mobility can be related to the sequence, given that this is the sole differentiating factor. We employed this advantage to detect each target in the background of guide oligos. Samples were run once.

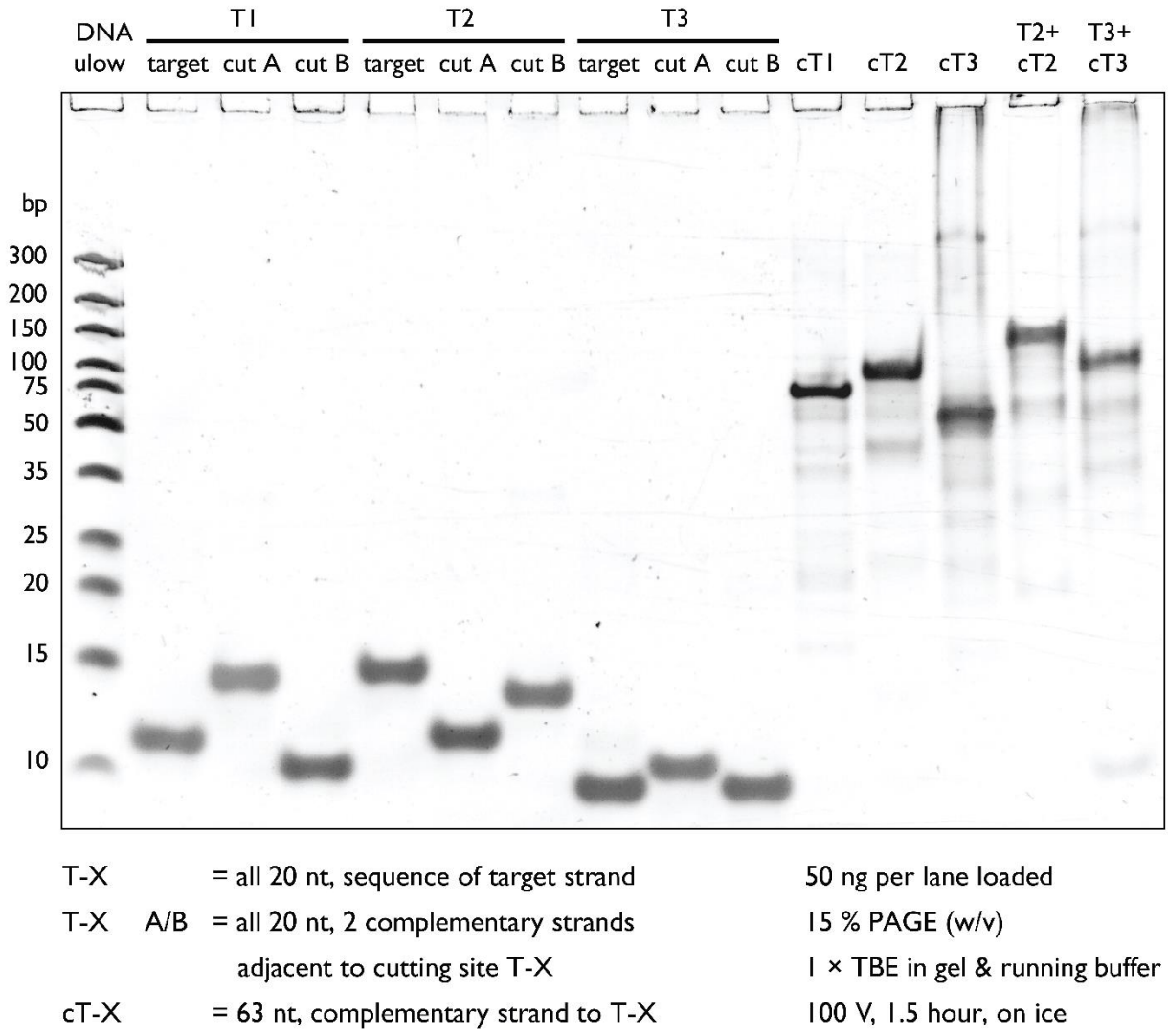

Figure S12. PAGE analysis of oligonucleotides used for MS2 RNase H cutting, target strands, and complementary capture strands. Thermo Scientific™ GeneRuler Ultra Low Range DNA Ladder was used (DNA ulow). Samples were run once.

We performed a control PAGE analysis by treating MS2 RNA with RNase H cutting without guide oligos. Here, we tested if targets have significant binding to enzyme-treated RNA (Figure S13).

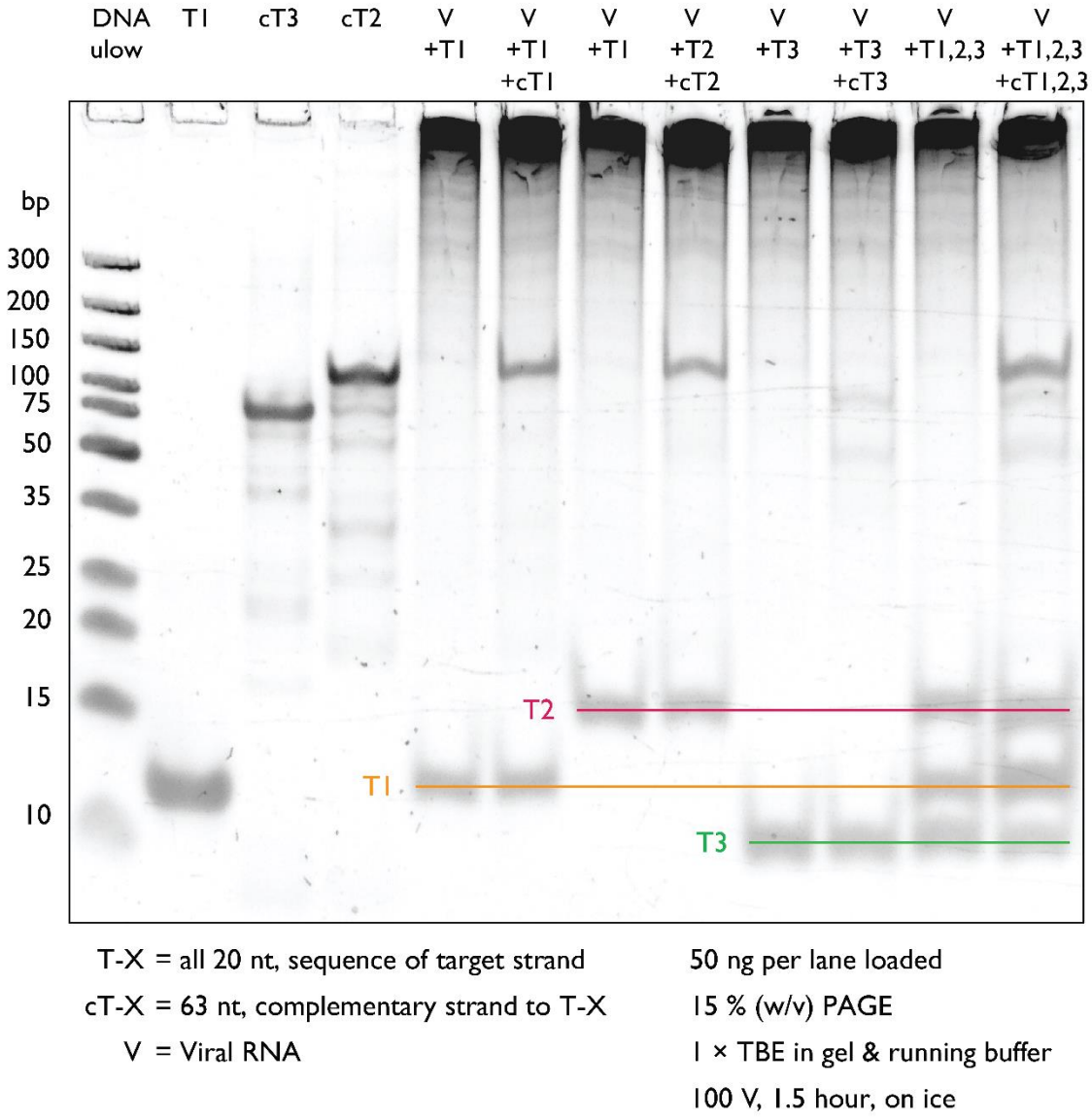

Figure S13. PAGE analysis of oligonucleotide mobility in a background of MS2 RNA treated with RNase H without added guide oligos. Samples were run once.

Previously, we have shown that MS2 RNA is cut in fragments of the desired size with 100 % efficiency. However, the release of target RNAs from cut MS2 RNA cannot be tested using this gel. In Figure S14 we tested if RNA target is free in solution. Once MS2 RNA is cut with one guide oligo, the target is absent (x T1A) and the T1A oligo is the only one visible. If both guide oligos are added for target T1 an additional band is visible on the gel. We wanted to validate that this band is the T1 target. This is performed by mixing cut MS2 with a complementary strand (cT1+30 T; the sequence is listed in Table S23) and observing a shift from the cT1+30 T strand.

In the case of the T2 target, we have not observed any additional band indicating that target M2 is probably bound to its position in MS2 RNA structure, as discussed in the main text.

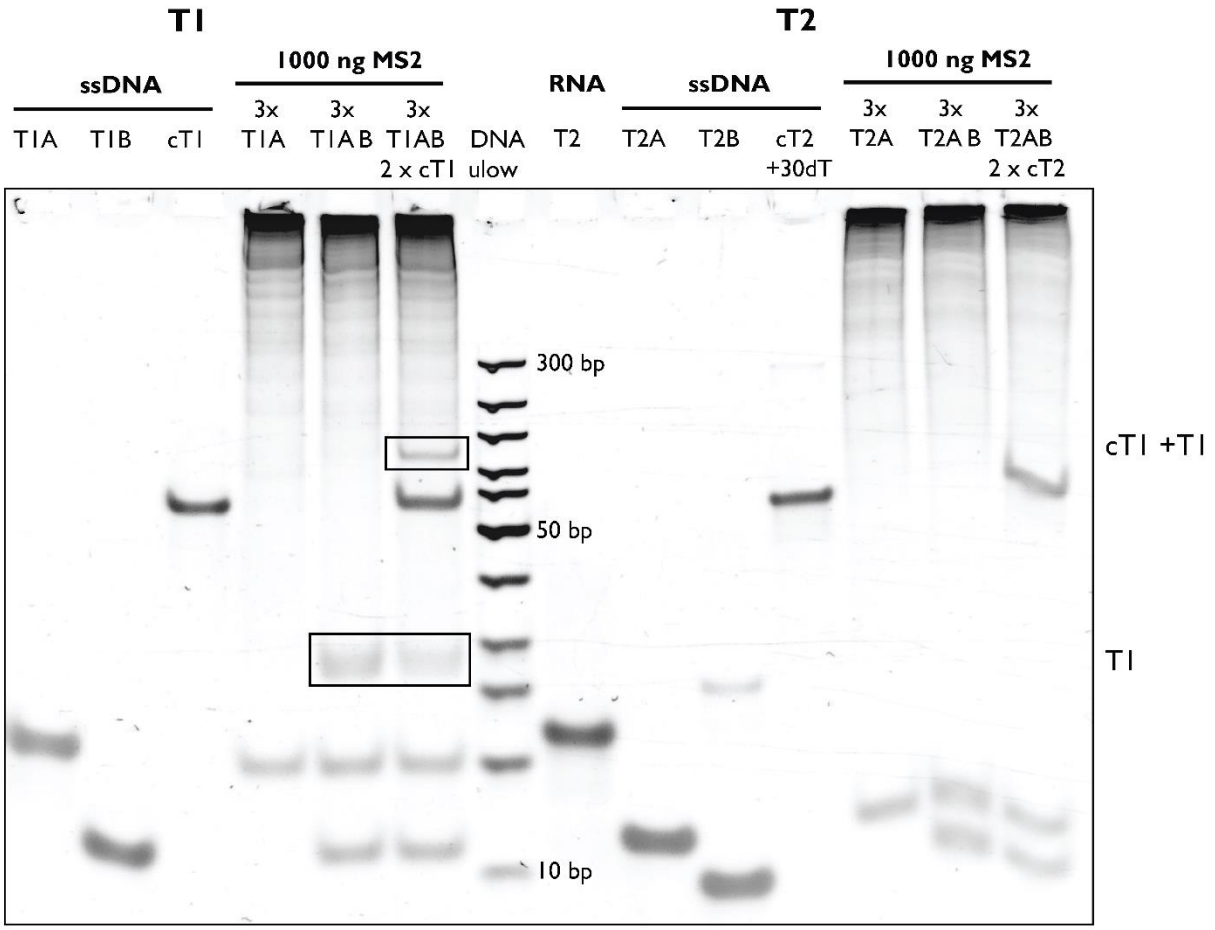

T-X = all 20 nt, sequence of target strand

T-X A/B = all 20 nt, 2 complementary strands adjacent to cutting site T-X

cT-X(+30 dT) = 63 nt, complementary strand to T-X

RNA M2	50 ng
T-X A & B	50 ng
cT-X	30 ng
MS2	1000 ng

15 % (w/v) PAGE

1 × TBE in gel & running buffer

100 V, 1.5 hour, on ice

Figure S14. PAGE analysis of target detection after MS2 RNA is treated with RNase H with respective guide oligos for targets T1 and T2 added. DNA ulow lane corresponds to GeneRuler Uultra Low Range DNA ladder (Thermo Fisher Scientific) with the lowest band being 10 bp and the highest band being 300 bp in length. Samples were run once.

Section S11. DNA nanobait for MS2 RNA target detection

Nanobait for MS2 virus is prepared as previously described in Section S2. Below are listed sequences of capture sites (Table S21), biotin strand (Table S20), and target sequence (Table S19). In Table S22 are listed guide oligos for all targets.

We also show additional nanopore events of nanobait without cut MS2 (Figure S15a), and with cut MS2 RNA added (Figure S15b). The nanobait and peaks resemble those presented in Figure 4b of the manuscript. These single-molecule events are obtained from three separate nanopore measurements.

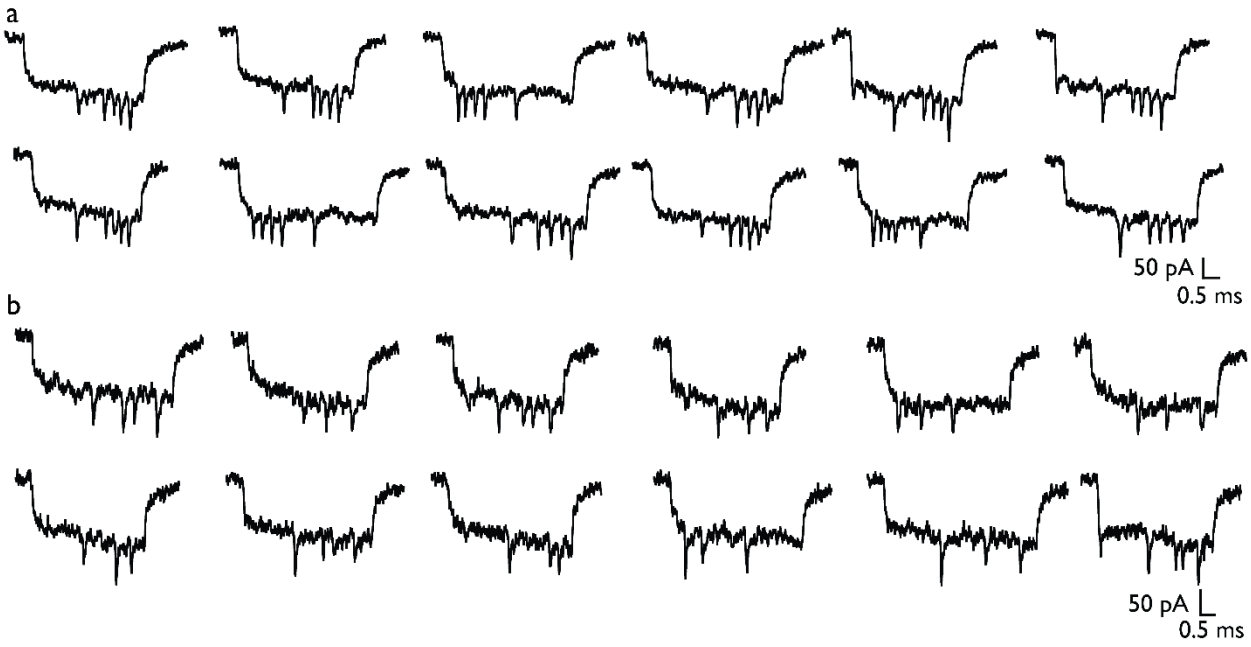

Figure S15. Example events for nanobait with cut MS2 RNA. a) Single-molecule nanobait events indicate that a) all three peaks are present, hence targets are not present, or b) peaks are absent, hence targets are present.

Supplementary Table S18. Presence of peaks at their respective sites for multiple MS2 viral target identification.

Target/Case	Control (no targets)	Standard error	Target present	Standard error
T1	0.08	0.01	0.41	0.01

T2	0.11	0.04	0.25	0.04
T3	0.06	0.03	0.14	0.02

Supplementary Table S19. Target sequences for MS2 target identification.

Strand name	Sequence (5' → 3')
T1	ACCACTAATGAGTGATATCC
T2	TACCTGTAGGTAACATGCTC
T3	TCTGCATCCGATTCCATCTC

Supplementary Table S20. 3' Biotinylated strand sequences for MS2 target identification.

Strand name	Sequence (5' → 3')	Length (nt)
bT1	AATGAGTGATATCC/3'-biotin/	14
bT2	TAGGTAACATGCTC/3'-biotin/	14
bT3	TCCGATTCCATCTC/3'-biotin/	14

Supplementary Table S21. Capture strand sequences for MS2 target identification.

Strand name	Sequence (5' → 3')
cT1_42	TTCGACAACTCGTATTAAATCCTTTGCCCGAACGTTATTTTTT GGATATCACTCATTAGTGGT
cT2_55	GTGAGTGAATAACCTTGCTTCTGTAAATCGTCGCTATT TTTTT GAGCATGTTACCTACAGGTA
cT3_68	AGAATATAAAGTACCGACAAAAGGTAAAGTAATTCTGT TTTTT GAGATGGAATCGGATGCAGA

Supplementary Table S22. Guide oligo sequences for MS2 target identification.

Strand name	Sequence (5’ → 3’)
T1a	AACCAACCGAACTGCAACTC
T1b	AAGCATCTCATATGCACCCT
T2a	GGAGCCAGTCGACAACGAAT
T2b	ACGGGGGCCGTAAGGCCCTC
T3a	CGATAAGTCTATCGTCGCAA
T3b	AACTCCACACCAGGCGATCG

Supplementary Table S23. Complementary strands to MS2 targets with the 30 T-tail used for PAGE gel analysis.

Strand name	Sequence (5’ → 3’)
cM1_30T	TTTTTTTTTTTTTTTTTTTTTTTTTTTTTTGGATATCACTCATTAGTGGT
cM2_30T	TTTTTTTTTTTTTTTTTTTTTTTTTTTTTTGAGCATGTTACCTACAGGTA

Section S12. Detection of SARS-CoV-2 RNA targets from patient samples using DNA nanobait

Nanobait for SARS-CoV-2 virus is prepared as previously described in Section S2. Below are listed sequences of capture sites (Table S26), biotin strand (Table S25), and target sequence (Table S24). In Table S27 are listed guide oligos for all targets.

Supplementary Table S24. Target sequences for SARS-CoV-2 target identification in a patient sample.

Strand name	Sequence (5' → 3')
S1	CATCCTTACTGCGCTTCGAT
S2	CATTGCAACTGAGGGAGCCT
S3	AGACTCAGACTAATTCTCCT

Supplementary Table S25. 3' Biotinylated strand sequences for SARS-CoV-2 target identification in a patient sample.

Strand name	Sequence (5' → 3')	Length (nt)
bS1	TACTGCGCTTCGAT/3'-biotin/	14
bS2	AACTGAGGGAGCCT/3'-biotin/	14
bS3	AGACTAATTCTCCT/3'-biotin/	14

Supplementary Table S26. Capture strand sequences for SARS-CoV-2 target identification in a patient sample.

Strand name	Sequence (5' → 3')
cS1_43	TTCGACAACTCGTATTAAATCCTTTGCCCGAACGTTAT TTTTT ATCGAAGCGCAGTAAGGATG

cS2_55	GTGAGTGAATAACCTTGCTTCTGTAAATCGTCGCTATT TTTTT AGGCTCCCTCAGTTGCAATG
cS3_68	AGAATATAAAGTACCGACAAAAGGTAAAGTAATTCTGT TTTTT AGGAGAATTAGTCTGAGTCT

Supplementary Table S27. Guide DNA oligo sequences for SARS-CoV-2 target identification in patient samples.

Strand name	**Sequence (5' → 3')**
S1a	GCTAGTGTAACTAGCAAGAA
S1b	ATTGCAGCAGTACGCACACA
S2a	CGTTCTCCATTCTGGTTACT
S2b	GTGATCTTTTGGTGTATTCA
S3a	GATAACTAGCGCATATACCT
S3b	GCTACACTACGTGCCCGCCG

Section S13. Detection of SARS-CoV-2 RNA targets from patient samples using DNA nanobait and DNA flower as a label

The nanobait synthesis follows the previously presented protocol including RNase H cutting and the SDR. As shown in Figure S16, to construct the reference structures on the nanobait, staples 26-32 and 96-102 were substituted by the relevant dumbbell sequences (Table S29). To link the DNA flowers onto the nanobait, staple 43 was substituted by strand P43 and C43 (C43 was added during preparation of 7WJa, so only P43 was added), staple 57 was substituted by strand C57 and P57, and staple 68 was substituted by strand cS3-68. The staples were mixed, and then the linear M13 scaffold was added into the solution (20 nM M13 scaffold, 60 nM staples, 120 nM dumbbell strands, and 120 nM P43, C57, P57, cS3-68). The mixture was heated to 70 °C followed by a linear cooling ramp to 25 °C over 50 minutes. 1 μL of 4 μM 7WJa, 7WJb, and 7WJc (DNA flowers) were added into the 40 μL nanobait solution and incubated at room temperature for 2 h. Finally, the resulted solution was diluted with a washing buffer (10 mM Tris-HCl, 0.5 mM $MgCl_2$, pH 8.0) to 500 μL and centrifuged at 6000 × g for 10 min with an Amicon Ultra 100 kDa filter to remove the excess DNA strands and DNA flowers (repeated 3 times). About 35 μL of nanobait solution was obtained and quantified with a NanoDrop 2000 spectrophotometer.

The flower nanobait for the COVID-19 patient sample was diluted to 250 pM. 3.8 μL of a patient sample (positive or negative samples were processed by the programmable RNase H cutting step) was mixed with 0.2 μL of 250 pM nanobait, 0.5 μL of 100 mM $MgCl_2$, and 0.5 μL of 1 M NaCl. The mixture (5 μL) was incubated at room temperature for 10 min and then diluted by 5 μL of 8 M LiCl and 20 μL of 4 M LiCl (in 1 × TE, pH 9.0) proceeding the nanopore measurement.

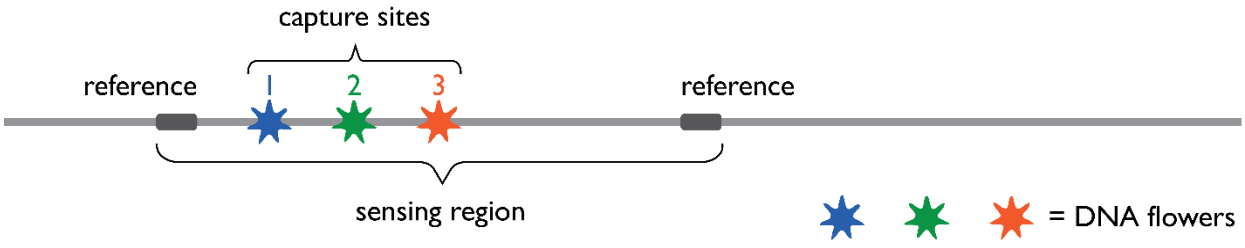

Figure S16. Design of nanobait with the DNA flower labels for testing COVID-19 patient sample. Each of the references is represented by eleven closely spaced DNA dumbbells.

Oligonucleotide sequences for DNA flower-based detection with nanobait are listed in Table S28. Example events for negative and positive SARS-CoV-2 patient samples obtained using DNA flowers are shown in Figure S17a and Figure S17b, respectively.

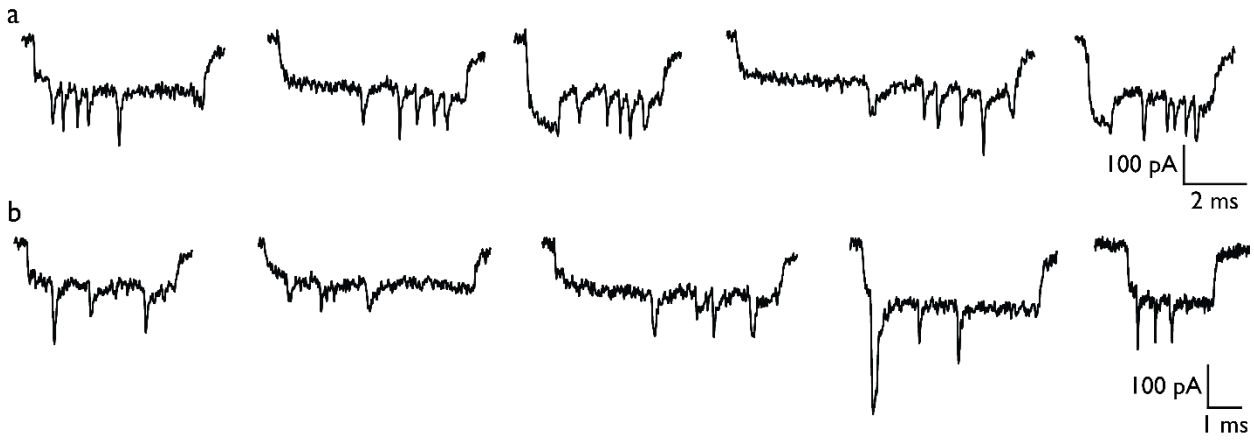

Figure S17. Example events of nanobait with DNA flower labels incubated with negative and positive SARS-CoV-2 patient samples (a and b, respectively).

Supplementary Table S28. Capture strand sequences for SARS-CoV-2 target identification in a patient sample using DNA flower as a label.

Strand name	Replaced oligo #	Sequence (5' → 3')
cFS1_43	43	TAATTTTAAAAGTTTGAGTA TT ATCGAAGCGCAGTA AGGATG
43+	43	ACATTATCATTTTGCGGA
cFS2_57	57	AGCTTAGATTAAGACGCTGA TT AGGCTCCCTCAGTT GCAATG
57+	57	GAAGAGTCAATAGTGAAT
cFS3_68	68	AGAATATAAAGTACCGACAAAAGGTAAAGTAATTCTGT TTTTT AGGAGAATTAGTCT GAGTCT

Supplementary Table S29. List of oligonucleotides that were replaced from Table S2 to assemble reference structures for nanobait with DNA flower. DNA dumbbell forming sequence is indicated in red.

Strand name	Sequence (5' → 3')	Length (nt)	Replaced oligo #
*REF 1.1	CTGAAAGCGTAAGAATACGTGGCACAGACAATATTTTTGAATGGCT	46	
*REF 1.2	ACATCACTTGTCCTCTTTTGAGGAACAAGTTTTCTTGTCCTGAGTAGA	48	
*REF 1.3	AGAACTCAAATCCTCTTTTGAGGAACAAGTTTTCTTGTCTATCGGCCT	48	
*REF 1.4	TGCTGGTAATTCCTCTTTTGAGGAACAAGTTTTCTTGTATCCAGAACA	48	
*REF 1.5	ATATTACCGCTCCTCTTTTGAGGAACAAGTTTTCTTGTCAGCCATTGC	48	
*REF 1.6	AACAGGAAAATCCTCTTTTGAGGAACAAGTTTTCTTGTACGCTCATGG	48	26-32
*REF 1.7	AAATACCTACTCCTCTTTTGAGGAACAAGTTTTCTTGTATTTTGACGC	48	
*REF 1.8	TCAATCGTCTTCCTCTTTTGAGGAACAAGTTTTCTTGTGAAATGGATT	48	
*REF 1.9	ATTTACATTGTCCTCTTTTGAGGAACAAGTTTTCTTGTGCAGATTCAC	48	
*REF 1.10	CAGTCACACGTCCTCTTTTGAGGAACAAGTTTTCTTGTACCAGTAATA	48	
*REF 1.11	AAAGGGACATTCCTCTTTTGAGGAACAAGTTTTCTTGTTCTGGCCAAC	48	
*REF 1.12	AGAGATAGAATCCTCTTTTGAGGAACAAGTTTTCTTGTCCCTTCTGAC	48	
*REF 2.1	CTTGAGCCATTCCTCTTTTGAGGAACAAGTTTTCTTGTTTGGGAATTA	48	
*REF 2.2	GAGCCAGCAATCCTCTTTTGAGGAACAAGTTTTCTTGTAATCACCAGT	20	
*REF 2.3	AGCACCATTATCCTCTTTTGAGGAACAAGTTTTCTTGTCCATTAGCAA	48	96-102
*REF 2.4	GGCCGGAAACTCCTCTTTTGAGGAACAAGTTTTCTTGTGTCACCAATG	48	
*REF 2.5	AAACCATCGATCCTCTTTTGAGGAACAAGTTTTCTTGTTAGCAGCACC	48	
*REF 2.6	GTAATCAGTATCCTCTTTTGAGGAACAAGTTTTCTTGTGCGACAGAAT	48	

*REF 2.7	CAAGTTTGCCTCCTCTTTTGAGGAACAAGTTTTCTTGTTTTAGCGTCA	48
*REF 2.8	GACTGTAGCGTCCTCTTTTGAGGAACAAGTTTTCTTGTCGTTTTCATC	48
*REF 2.9	GGCATTTTCGTCCTCTTTTGAGGAACAAGTTTTCTTGTGTCATAGCCC	48
*REF 2.10	CCTTATTAGCTCCTCTTTTGAGGAACAAGTTTTCTTGTGTTTGCCATC	48
*REF 2.11	TTTTCATAATTCCTCTTTTGAGGAACAAGTTTTCTTGTCAAAATCACC	48
*REF 2.12	GGAACCAGAGCCACCACCGGAACCGCCTCCCTCAGAGCCGCCACCC	46

Section S14. Nanopore data analysis

Data analysis of nanopore current traces is performed as previously described [1,4,16]. The data analysis workflow is shown in Figure S18. Firstly, in a raw ionic current trace, our home-built LabView script identifies events by specifying the event duration range and the current threshold. In the next step, nanobait events are separated from isolated events with too small and too large event charge deficit (ECD). Nanobaits can translocate through the nanopore as unfolded or folded (Figure S18). Downward peaks were identified as described previously[1]. The key advantage of nanobait is its pre-determined design relying on the identification of unique current signatures[1,17]. A specific current drop threshold correlating to approximately double the baseline noise was used to identify peaks. Firstly, the reference peaks are identified and positioned. Next, the presence of the peaks corresponding to our sensing sites was identified and an appropriate color was assigned. Lastly, we determine present peaks and calculate displacement efficiency for each site.

Nanopore events can be analyzed with the convolutional neural network QuipuNet following the procedure outlined in Figure S18. Its event detection is much faster, with the rate of 1600 events/s, making it appropriate for instantaneous, real-time data analysis[16] that is not achievable with the other detection methods[18–20].

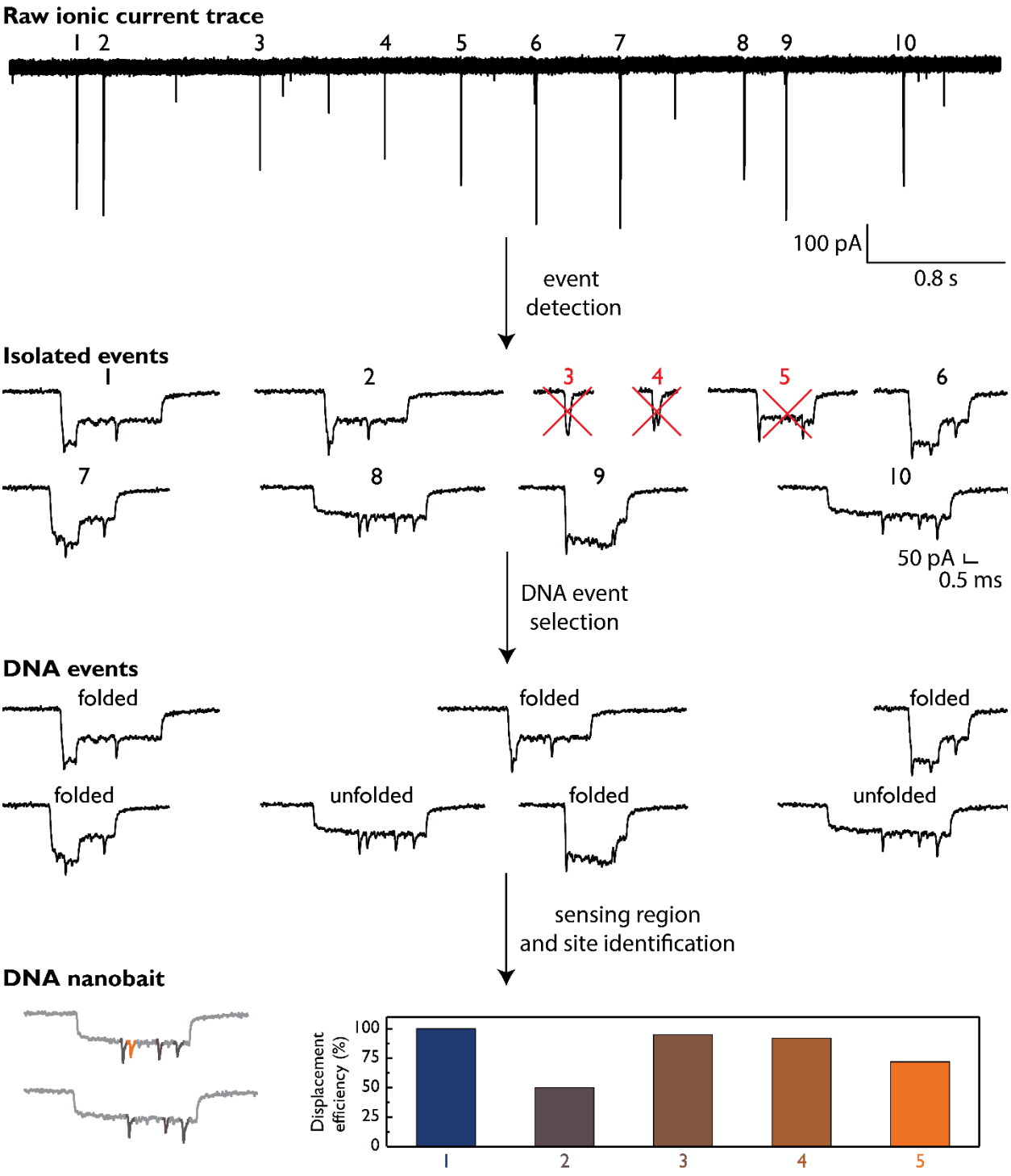

Figure S18. Nanopore data analysis workflow. The data analysis starts by searching for single-molecule events from the raw nanopore ionic current traces. Event's duration, current drop, and event charge deficit (ECD i.e. event's surface area) are parameters that further separate nanobait events from DNA events. DNA events in nanopore measurements can include bent or folded

events and linear or unfolded events. The next analysis step includes identifying the sensing region (marked by two references) and the absence of the peaks at their respective sites. In the last step, we calculate the mean and errors from multiple single-molecule events (from multiple nanopores), that are subtracted to the control measurement and presented as the displacement efficiency in the bar chart.

Section S15. Nanopore statistics

Nanopore measurements are listed in Table S30 with characteristics of both nanopores used and sample presented. In all measurements, the first fifty unfolded nanobaits were used for the displacement efficiency calculations unless otherwise specified. All measurements were obtained under an applied field of 600 mV and the respective ionic current value is indicated in Table S30. Only nanopores with the linear current-voltage curve and the noise root mean square (RMS) of < 7 pA were used for nanopore measurements.

Supplementary Table S30. Nanopore measurement details for all experiments presented in this study.

Nanopore measurement	DNA nanobait type / sample name	Current at 600 mV (nA)	Target present	RNase H cutting	Human total RNA	Patient sample	Excess of targets (times)	Incubation time (min)
1	Blank	10	/	/	/	/	10	10
2	Blank	11	/	/	/	/	10	10
3	Blank	14.5	/	/	/	/	10	10
4	Blank	14	/	/	/	/	10	10
5	Blank	11	/	/	/	/	10	10
6	Blank	7	/	/	/	/	10	10
7	Blank	12	/	/	/	/	10	10
8	Blank	8	/	/	/	/	10	10
9	H1-H5	12.4	five targets	/	/	/	10	10
10	H1-H5	9.8	five targets	/	/	/	10	10
11	H1-H5	12.15	five targets	/	/	/	10	10
12	H1-H5	12.3	five targets	/	/	/	10	10
13	total RNA + Nanobait	9.5	/	/	yes	/	10	10
14	total RNA + Nanobait	10.2	/	/	yes	/	10	10
15	total RNA + Nanobait	10	/	/	yes	/	10	10
16	total RNA + Nanobait+targets	9.4	five targets	/	yes	/	10	10
17	total RNA + Nanobait+targets	9.25	five targets	/	yes	/	10	10
18	total RNA + Nanobait+targets	10.5	five targets	/	yes	/	10	10

19	Nanobait + negative covid sample a53	9	/	/	/	negative	NA	10
20	Nanobait + negative covid sample a53	9	/	/	/	negative	NA	10
21	Nanobait + negative covid sample a53	10.6	/	/	/	negative	NA	10
22	Nanobait + negative covid sample a55	10.2	/	/	/	negative	NA	10
23	Nanobait + negative covid sample a55	11	/	/	/	negative	NA	10
24	Nanobait + negative covid sample a55	8.72	/	/	/	negative	NA	10
25	Nanobait + negative covid sample+targets	10.5	/	/	/	negative	NA	10
26	Nanobait + negative covid sample+targets	10.25	/	/	/	negative	NA	10
27	Nanobait + negative covid sample+targets	11	/	/	/	negative	NA	10
28	Nanobait + negative covid sample+RNaseH cutting	10.2	/	yes	/	negative	NA	10
29	Nanobait + negative covid sample+RNaseH cutting	9.8	/	yes	/	negative	NA	10
30	kinetics 1 min DNA	9.8	all targets	/	/	/	10	1
31	kinetics 2.5 min DNA	10.9	all targets	/	/	/	10	2.5
32	kinetics 5 min DNA	11.2	all targets	/	/	/	10	5
33	kinetics 10 min DNA	10	all targets	/	/	/	10	10
34	kinetics 1 min RNA	12	all targets	/	/	/	10	1
35	kinetics 2.5 min RNA	12.4	all targets	/	/	/	10	2.5
36	kinetics 5 min RNA	12.2	all targets	/	/	/	10	5
37	kinetics 10 min RNA	10	all targets	/	/	/	10	10
38	Nanobait for MS2 blank	12	/	/	/	/	10	10
39	Nanobait for MS2 blank	11	/	/	/	/	10	10
40	Nanobait for MS2 blank	11	/	/	/	/	10	10
41	Nanobait for MS2 blank+targets	11.58	all targets	/	/	/	10	10
42	Nanobait for MS2 blank+targets	10.8	all targets	/	/	/	10	10

43	Nanobait for MS2 blank+RNaseH cutting	10	/	yes	/	/	10	10
44	Nanobait for MS2 blank+RNaseH cutting	12.5	/	yes	/	/	10	10
45	Nanobait for MS2 blank+RNaseH cutting	13.1	/	yes	/	/	10	10
46	Nanobait for a patient covid sample	11	/	/	/	/	10	10
47	Nanobait for a patient covid sample	10.7	/	/	/	/	10	10
48	Nanobait for patient covid sample+negative sample	9.9	/	yes	/	negative	NA	10
49	Nanobait for patient covid sample+positive sample	9.8	/	yes	/	positive	NA	10
50	Nanobait for patient covid sample+positive sample	10.7	/	yes	/	positive	NA	10
51	Nanobait for patient covid sample+positive sample	10.4	/	yes	/	positive	NA	10
52	Nanobait for patient covid sample with DNA flower	6.98	/	/	/	/	10	10
53	Nanobait for patient covid sample with DNA flower+negative sample	11.4	/	yes	/	negative	NA	10
54	Nanobait for patient covid sample with DNA flower+negative sample	11.18	/	yes	/	negative	NA	10
55	Nanobait for patient covid sample with DNA flower	11.44	/	yes	/	positive	NA	10
56	Nanobait for patient covid sample with DNA flower	9.89	/	yes	/	positive	NA	10
57	Nanobait for patient covid sample with DNA flower	10.1	/	yes	/	positive	NA	10
58	Nanobait for multiple viruses blank	9	/	/	/	/	10	10

59	Nanobait for multiple viruses blank	7.5	/	/	/	/	10	10
60	Nanobait for multiple viruses blank	8.5	/	/	/	/	10	10
61	Nanobait for multiple viruses blank+all targets	8.8	all targets	/	/	/	10	10
62	Nanobait for multiple viruses blank+all targets	8	all targets	/	/	/	10	10
63	Nanobait for multiple viruses blank+all targets	11	all targets	/	/	/	10	10
64	Nanobait for multiple viruses blank+SARS-CoV-2 target	8.6	SARS-CoV-2	/	/	/	10	10
65	Nanobait for multiple viruses blank+SARS-CoV-2 target	10.15	SARS-CoV-2	/	/	/	10	10
66	Nanobait for multiple viruses blank+SARS-CoV-2 target	11.4	SARS-CoV-2	/	/	/	10	10
67	Nanobait for multiple viruses blank+Influenza target	8.99	Influenza	/	/	/	10	10
68	Nanobait for multiple viruses blank+Influenza target	9.42	Influenza	/	/	/	10	10
69	Nanobait for multiple viruses blank+Influenza target	14.8	Influenza	/	/	/	10	10
70	Nanobait for multiple viruses blank+RSV target	9.54	RSV	/	/	/	10	10
71	Nanobait for multiple viruses blank+RSV target	15.15	RSV	/	/	/	10	10
72	Nanobait for multiple viruses blank+RSV target	9.3	RSV	/	/	/	10	10
73	Nanobait for multiple viruses blank+Parainfluenza target	9.6	Parainfluenza	/	/	/	10	10
74	Nanobait for multiple viruses	9.67	Parainfluenza	/	/	/	10	10

	blank+Parainfluenza target							
75	Nanobait for multiple viruses blank+Parainfluenza target	15.2	Parainfluenza	/	/	/	10	10
76	Nanobait for multiple viruses blank+Rhinoviruses target	8.9	Rhinoviruses	/	/	/	10	10
77	Nanobait for multiple viruses blank+Rhinoviruses target	15.5	Rhinoviruses	/	/	/	10	10
78	Nanobait for multiple viruses blank+Rhinoviruses target	9.74	Rhinoviruses	/	/	/	10	10
79	Nanobait for variants blank	9.01	/	/	/	/	10	10
80	Nanobait for variants blank	9.7	/	/	/	/	10	10
81	Nanobait for variants blank	8.52	/	/	/	/	10	10
82	Nanobait for variants blank + WT targets	8.5	all targets	/	/	/	10	10
83	Nanobait for variants blank + WT targets	8.5	all targets	/	/	/	10	10
84	Nanobait for variants blank + WT targets	7.8	all targets	/	/	/	10	10
85	Nanobait for variants blank + variant targets	8.8	all targets	/	/	/	10	10
86	Nanobait for variants blank + variant targets	9.03	all targets	/	/	/	10	10
87	Nanobait for variants blank + variant targets	9	all targets	/	/	/	10	10
88	Nanobait for variants+SARS-CoV-2 reference variant target	11.5	SARS-CoV-2 reference	/	/	/	10	10
89	Nanobait for variants+ SARS-CoV-2 reference variant target	10.5	SARS-CoV-2 reference	/	/	/	10	10
90	Nanobait for variants+ SARS-CoV-2 reference variant target	9.7	SARS-CoV-2 reference	/	/	/	10	10

91	Nanobait for variants+Delta variant target	10	Delta	/	/	/	10	10
92	Nanobait for variants+Delta variant target	10	Delta	/	/	/	10	10
93	Nanobait for variants+Delta variant target	12	Delta	/	/	/	10	10
94	Nanobait for variants+ B.1 variant target	10.1	B.1	/	/	/	10	10
95	Nanobait for variants+ B.1 variant target	13.75	B.1	/	/	/	10	10
96	Nanobait for variants+ B.1 variant target	12.8	B.1	/	/	/	10	10
97	Nanobait for variants+Alpha variant target	10.68	Alpha	/	/	/	10	10
98	Nanobait for variants+Alpha variant target	8.3	Alpha	/	/	/	10	10
99	Nanobait for variants+Alpha variant target	11.3	Alpha	/	/	/	10	10
100	Nanobait for variants+Beta variant target	9.5	Beta	/	/	/	10	10
101	Nanobait for variants+Beta variant target	9.7	Beta	/	/	/	10	10
102	Nanobait for variants+Beta variant target	14.1	Beta	/	/	/	10	10
103	Nanobait for patient covid sample+negative sample	11	/	yes	/	negative	NA	10
104	Nanobait for patient covid sample+negative sample	12	/	yes	/	negative	NA	10
105	Nanobait for patient covid sample+negative sample	9.7	/	yes	/	negative	NA	10
106	Nanobait for patient covid sample+negative sample	11	/	yes	/	negative	NA	10
107	Nanobait for patient covid	11.5	/	yes	/	negative	NA	10

	sample+negative sample							
108	Nanobait for patient covid sample+negative sample	10	/	yes	/	negative	NA	10
109	Nanobait for patient covid sample+negative sample	11.1	/	yes	/	negative	NA	10
110	Nanobait for patient covid sample+negative sample	11.3	/	yes	/	negative	NA	10
111	Nanobait for patient covid sample+negative sample	11.8	/	yes	/	negative	NA	10
112	Nanobait for SARS-CoV-2 RNA N501	7	/	/	/	/	10	10
113	Nanobait for SARS-CoV-2 RNA N501+wild-type	8.36	WT	yes	/	/	10	10
114	Nanobait for SARS-CoV-2 RNA N501+wild-type	7.6	WT	yes	/	/	10	10
115	Nanobait for SARS-CoV-2 RNA N501+wild-type	5.6	WT	yes	/	/	10	10
116	Nanobait for SARS-CoV-2 RNA N501+N501S	12.78	N501S	yes	/	/	10	10
117	Nanobait for SARS-CoV-2 RNA N501+ N501S	8.7	N501S	yes	/	/	10	10
118	Nanobait for SARS-CoV-2 RNA N501+ N501S	9	N501S	yes	/	/	10	10
119	Nanobait for SARS-CoV-2 RNA N501+N501T	12.6	N501T	yes	/	/	10	10
120	Nanobait for SARS-CoV-2 RNA N501+ N501T	8.2	N501T	yes	/	/	10	10
121	Nanobait for SARS-CoV-2 RNA N501+ N501T	14	N501T	yes	/	/	10	10

Section S16. Sensitivity curve

We prepared serial dilutions of nanobait with SARS-CoV-2 N501 WT cut RNA (Figure S19a; details in Section S8). Any contact surfaces were passivated with a 20 bp DNA (5 nM; 5'-GACCACTACAGTTGTAATCC-3' IDT) prior to contact with the diluted samples to prevent surface binding. The sensitivity curve was shown from fM to nM range of nanobait concentrations.

Nanobait was mixed with SARS-CoV-2 RNA targets (20 nt, H2 and H5 sequences in Supplementary Table S15) in various ratios of RNA for 10 min and by keeping nanobait concentration constant (Figure S19b).

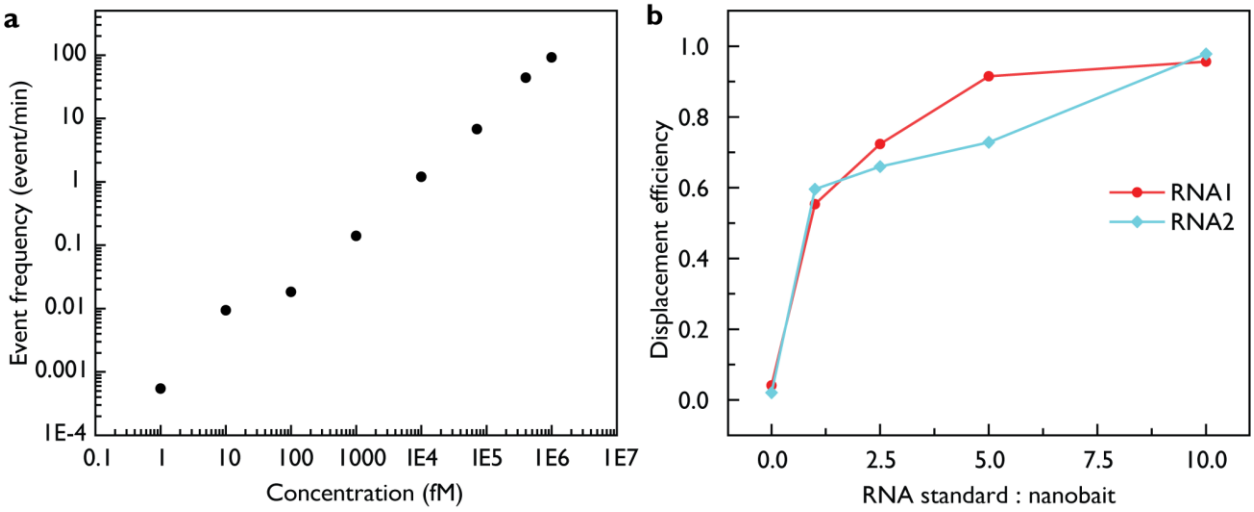

Figure S19. Sensitivity curve of nanobait-nanopore system. **a)** Nanobait detection with SARS-CoV-2 N501 wild-type target as described in Section S8. Were detected in the range from femtomolar (fM) to nanomolar (nM) concentrations. Event frequency was plotted as a function of log of nanobait concentration in fM versus log of event frequency in events per min. **b)** Nanobait displacement efficiency with variable SARS-CoV-2 RNA concentrations. Nanobait concentration was constant at 500 pM and viral RNAs (RNA1 and RNA2 correspond to H2 and H4, respectively; 20 nt) were varied from 1:1 ratio to 1:10 excess to nanobait to test dynamic range of nanobait.

REFERENCES

1. Bell, N. A. W. & Keyser, U. F. Digitally encoded DNA nanostructures for multiplexed, single-molecule protein sensing with nanopores. *Nature Nanotechnology* **11**, 645–651 (2016).

2. Stahl, E., Martin, T. G., Praetorius, F. & Dietz, H. Facile and Scalable Preparation of Pure and Dense DNA Origami Solutions. *Angewandte Chemie International Edition* **53**, 12735–12740 (2014).

3. Ohmann, A. *et al.* Controlling aggregation of cholesterol-modified DNA nanostructures. *Nucleic Acids Res* **47**, 11441–11451 (2019).

4. Bošković, F., Ohmann, A., Keyser, U. F. & Chen, K. DNA Structural Barcode Copying and Random Access. *Small Structures* **2**, 2000144 (2021).

5. Chen, K., Zhu, J., Bošković, F. & Keyser, U. F. Nanopore-based dna hard drives for rewritable and secure data storage. *Nano Letters* **20**, 3754–3760 (2020).

6. Fairhead, M., Krndija, D., Lowe, E. D. & Howarth, M. Plug-and-Play Pairing via Defined Divalent Streptavidins. *Journal of Molecular Biology* **426**, 199–214 (2014).

7. Zhu, J., Ermann, N., Chen, K. & Keyser, U. F. Image Encoding Using Multi-Level DNA Barcodes with Nanopore Readout. *Small* **17**, 2100711 (2021).

8. Schindelin, J. *et al.* Fiji: An open-source platform for biological-image analysis. *Nature Methods* **9**, 676–682 (2012).

9. Lu, X. *et al.* Real-time reverse transcription-PCR assay for comprehensive detection of human rhinoviruses. *Journal of Clinical Microbiology* **46**, 533–539 (2008).

10. Templeton, K. E., Scheltinga, S. A., Beersma, M. F. C., Kroes, A. C. M. & Claas, E. C. J. Rapid and Sensitive Method Using Multiplex Real-Time PCR for Diagnosis of Infections by Influenza A and Influenza B Viruses, Respiratory Syncytial Virus, and Parainfluenza Viruses 1, 2, 3, and 4. *Journal of Clinical Microbiology* **42**, 1564–1569 (2004).

11. Wu, F. *et al.* A new coronavirus associated with human respiratory disease in China. *Nature* **579**, 265–269 (2020).

12. https://www.who.int/influenza/gisrs_laboratory/WHO_information_for_the_molecular_detection_of_influenza_viruses_20171023_Final.pdf.

13. Shirato, K. *et al.* Diagnosis of human respiratory syncytial virus infection using reverse transcription loop-mediated isothermal amplification. *Journal of Virological Methods* **139**, 78–84 (2007).

14. Konings, F. *et al.* SARS-CoV-2 Variants of Interest and Concern naming scheme conducive for global discourse. *Nature Microbiology* **6**, 821–823 (2021).

15. Rambaut, A. *et al.* A dynamic nomenclature proposal for SARS-CoV-2 lineages to assist genomic epidemiology. *Nature Microbiology* **5**, 1403–1407 (2020).

16. Misiunas, K., Ermann, N. & Keyser, U. F. QuipuNet: Convolutional Neural Network for Single-Molecule Nanopore Sensing. *Nano Letters* **18**, 4040–4045 (2018).

17. Bošković, F. & Keyser, U. F. Nanopore microscope identifies RNA isoforms with structural colors. *bioRxiv* 2021.10.16.464631 (2021) doi:10.1101/2021.10.16.464631.

18. Europe, W. H. Organization. R. O. for. Methods for the detection and identification of SARS-CoV-2 variants. *World Health Organization. Regional Office for Europe* (2021) doi:10.1002/9781119650034.ch16.

19. Caliendo, A. M. Multiplex PCR and emerging technologies for the detection of respiratory pathogens. *Clinical Infectious Diseases* **52**, 326–330 (2011).

20. Zhou, L. *et al.* Programmable low-cost DNA-based platform for viral RNA detection. *Science Advances* **6**, eabc6246 (2020).